Current Research (2020) Newfoundland and Labrador Department of Natural Resources Geological Survey, Report 20-1, pages 179-205

THE YELLOW FOX SHOWING: MONZOGRANITE-HOSTED, FRACTURE RELATED ANTIMONY–SILVER–GOLD MINERALIZATION NEAR THE EASTERN MARGIN OF THE MOUNT PEYTON INTRUSIVE SUITE, CENTRAL NEWFOUNDLAND (NTS MAP AREA 2D/14)

H.A.I. Sandeman and C. Spurrell[1]
Mineral Deposits Section
[1]Present address: Vale Canada Inc., 140 Nickel Road, Thompson, MN, Canada

ABSTRACT

The Yellow Fox showing is located 13 km southwest of Glenwood and was discovered in 2011 through grass-roots prospecting. It is hosted by monzogranite of the Late Silurian to Early Devonian Mount Peyton intrusive suite, central Newfoundland, and lies 1.8 km west of the inferred position of the southern extension of the Dog Bay Line. Sparse regional bedrock outcrops and five mineral-exploration-industry trenches demonstrate that the showing is hosted by fractured, muscovite–pyrite–rutile-altered, medium-grained, plagioclase porphyritic, granophyric-textured biotite ± hornblende monzogranite. Muscovite–pyrite–rutile alteration occurs in an approximately 100-m-long by 30-m-wide, broadly north-trending bleached and rusty zone, characterized by three distinct fracture sets. The most prominent fracture set is north-trending (356°/80°E), occurs on a spacing of 5–20 cm, and is accompanied by abundant muscovite and disseminated pyrite. A less common, metre-spaced, east-striking (098°/84°S) fracture set is barren with respect to alteration minerals or mineralization, whereas a third, weakly developed, north-northeast-trending (025°/86°E) fracture set, locally hosts a few narrow (<4 cm) stibnite–quartz–arsenopyrite veins. Arsenopyrite, mainly confined to vein margins, is extensively altered to supergene scorodite and goethite. The muscovite–pyrite–rutile alteration and north-trending fractures are cut by the north-northeast-trending stibnite–quartz–arsenopyrite-veined fractures. Relative to unaltered monzogranite, the early muscovite–pyrite–rutile-associated fracture set, and altered-host monzogranite samples, are typically moderately anomalous in As, Au, Ag, Sb, Pb and Cd. In contrast, the later stibnite–quartz–arsenopyrite-veined fractures and host rocks are strongly anomalous in all metals (Sb–As–Au–Ag–Pb–Zn–Cd) and weakly anomalous in Cu. No appreciable enrichment in Mo or W is evident. The host monzogranite is identical to other granites from the northeastern Mount Peyton intrusive suite, and all are weakly alkaline I- to A-type, biotite ± hornblende monzogranites. Mineralization must be younger than the ca. *419 Ma age of the monzogranite, may be contemporaneous with other intrusion-hosted mineralization in the area, and is probably Early Devonian. Fracturing and mineralization likely occurred in response to north-northwest-directed oblique sinistral Acadian deformation.*

INTRODUCTION

The Yellow Fox showing is located 13 km southwest of Glenwood in central Newfoundland (Figures 1 and 2; NTS map area 2D/14), and was discovered in 2011 by Metals Creek Resources Corporation during regional reconnaissance gold exploration (Reid and Myllyaho, 2012). The showing is poorly exposed because of the thick glacial till cover and the local landscape that consists mostly of gently undulating, till-mantled boggy ground covered by black spruce-dominated forest. Bedrock exposures are almost entirely restricted to sparse low bedrock ridges, stream beds and borrow pits constructed for forest-access road construction. The showing may be accessed using an all-terrain vehicle *via* a network of old logging roads.

The Yellow Fox showing occurs in the northeastern sector of the Mount Peyton map area, near the juncture of four 1:50 000-scale NTS map areas (2D/14, 15, 2E/03, 04), and 4.5 km south of the Corsair and Hurricane prospects and associated showings exposed along the Salmon River (Tallman, 1990; Evans, 1996; O'Driscoll and Wilton, 2005; Sandeman *et al.*, 2017; Figure 2). The showing is hosted by monzogranite of the Late Silurian to Early Devonian Mount Peyton intrusive suite (MPIS) of central Newfoundland (Blackwood, 1982; Dickson, 1993, 1996; Sandeman *et al.*, 2017), which is predominantly composed of gabbro, varying to diorite, and intruded by less voluminous monzogranite.

The Yellow Fox showing is located approximately 1.8 km west of the projected position of the southern extension

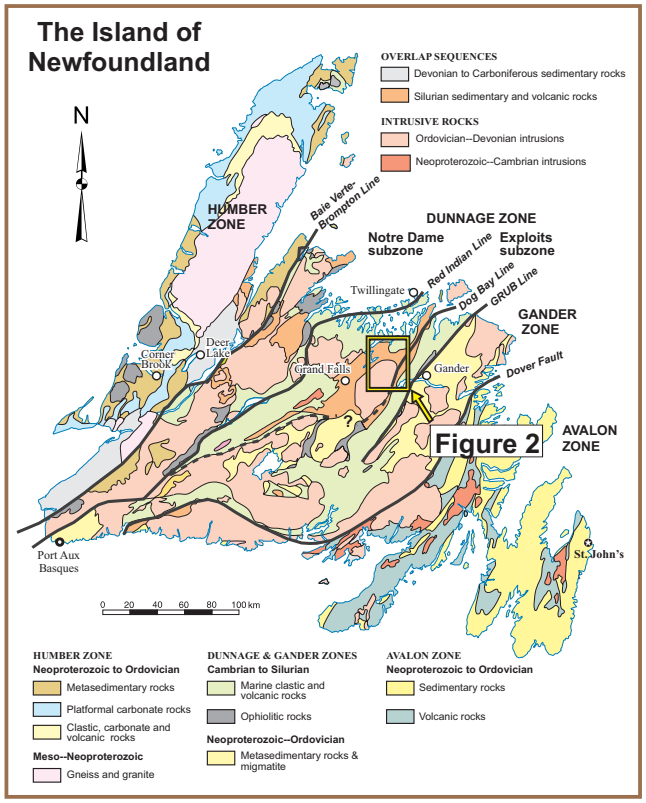

Figure 1. *Simplified geological map of the Island of Newfoundland showing the location of the Yellow Fox showing and Figure 2 with respect to major geological terranes and tectonic boundaries (after Colman-Sadd* et al.*, 1990).*

of the proposed terminal Iapetan suture, termed the Dog Bay Line (Currie, 1993; Piasecki, 1993; Williams, 1993; Williams *et al.*, 1993; Pollock *et al.*, 2007). East of the MPIS, and presumably constituting the most westerly unit lying southeast of the Dog Bay Line, lies the Silurian, shallow-marine, locally calcareous and macro-fossil-bearing siltstones and sandstones of the Indian Islands Group (Williams *et al.*, 1993; Currie, 1993, 1995; Dickson, 1993, 1996, 2006). These Silurian rocks are demonstrably imbricated with both Middle Ordovician siltstones and sandstone, and Late Ordovician graphitic, pyritic, and graptolitic shale (Sandeman *et al.*, 2018). Extensive mineral exploration work in the area has identified a number of precious-metal- and antimony-mineralized zones (Evans, 1996; Barbour and Churchill, 1999, 2004; O'Reilly *et al.*, 2010; Sandeman *et al.*, 2017, 2018) that may share common genetic attributes.

This report is a component of an ongoing, broader study of precious-metal mineralization in, and around, the MPIS and the Botwood and Indian Islands basins. These investigations build upon the extensive mapping, geochronology, biostratigraphy and lithogeochemical work of previous investigators (Dunning, 1992, 1994; Dunning and Manser, 1993; Dickson, 1993, 1994, 2006; Boyce and Ash, 1994; Dickson *et al.*, 2000, 2007; O'Brien, 2003; Boyce and Dickson, 2006; McNicoll *et al.*, 2006), as well as the more detailed mineral-deposit studies in the area (Evans and Wilson, 1994; Evans, 1996; O'Driscoll and Wilton, 2005; Squires, 2005; Lake and Wilton; 2006; Sandeman *et al.*, 2017, 2018), which collectively provide a framework upon which a better understanding of the mineralized systems of the region may be constructed. Herein, new field, petrographic and lithogeochemical data, along with Mineral Liberation Analysis (MLA) electron beam mapping and imagery, are presented for rocks of the Yellow Fox mineralized zone. Some of the data and observations presented herein formed the B.Sc. thesis of C. Spurrell at Memorial University of Newfoundland and Labrador (Spurrell, 2017). These data are supplemented by lithogeochemical data for granitic rocks of the region (Dickson and Kerr, 2007; Sandeman *et al.*, 2017) and are compared to available industry-assessment report data for the showing (Reid and Myllyaho, 2012) and to mineralized samples from the proximal, MPIS diorite-hosted Salmon River prospects (Tallman, 1990, 1991a; Hoffe and Sparkes, 2003; House, 2007a; Quinlan, 2009). The lithogeochemical data, along with field and petrographic observations on the style and character of alteration and additional observations from industry-assessment reports, enhance our collective knowledge-base for these intrusion-hosted precious-metal mineralized zones in the MPIS. These mineralized zones may share common genetic attributes with numerous proximal metasedimentary rock-hosted mineralized zones exposed east of the MPIS (*e.g.*, O'Driscoll and Wilton, 2005; Squires, 2005). Mineral abbreviations used herein are from Whitney and Evans (2010).

REGIONAL SETTING

The Yellow Fox showing lies in the northeastern Exploits Subzone of the Newfoundland Appalachians, and occurs 1.8 km west of the projected position of terminal Iapetan suture termed the Dog Bay Line (Figures 1 and 2; Currie, 1993; Piasecki, 1993; Williams, 1993; Williams *et al.*, 1993;

Figure 2. *(Figure on page 3) Geology of the northern part of the MPIS and adjacent country rocks illustrating the location of the Yellow Fox showing and its proximity to the projected southern extension of the Dog Bay Line as based on the detailed airborne geophysical data of Moore and Smith (2003) and House and McConnell (2003). The red dots are precious-metal showings taken from the Mineral Occurrence Database (MODS: gis.geosurv.gov.nl.ca/mods/mods.asp). Previous studied mineralization refers to those discussed in Sandeman* et al. *(2017).*

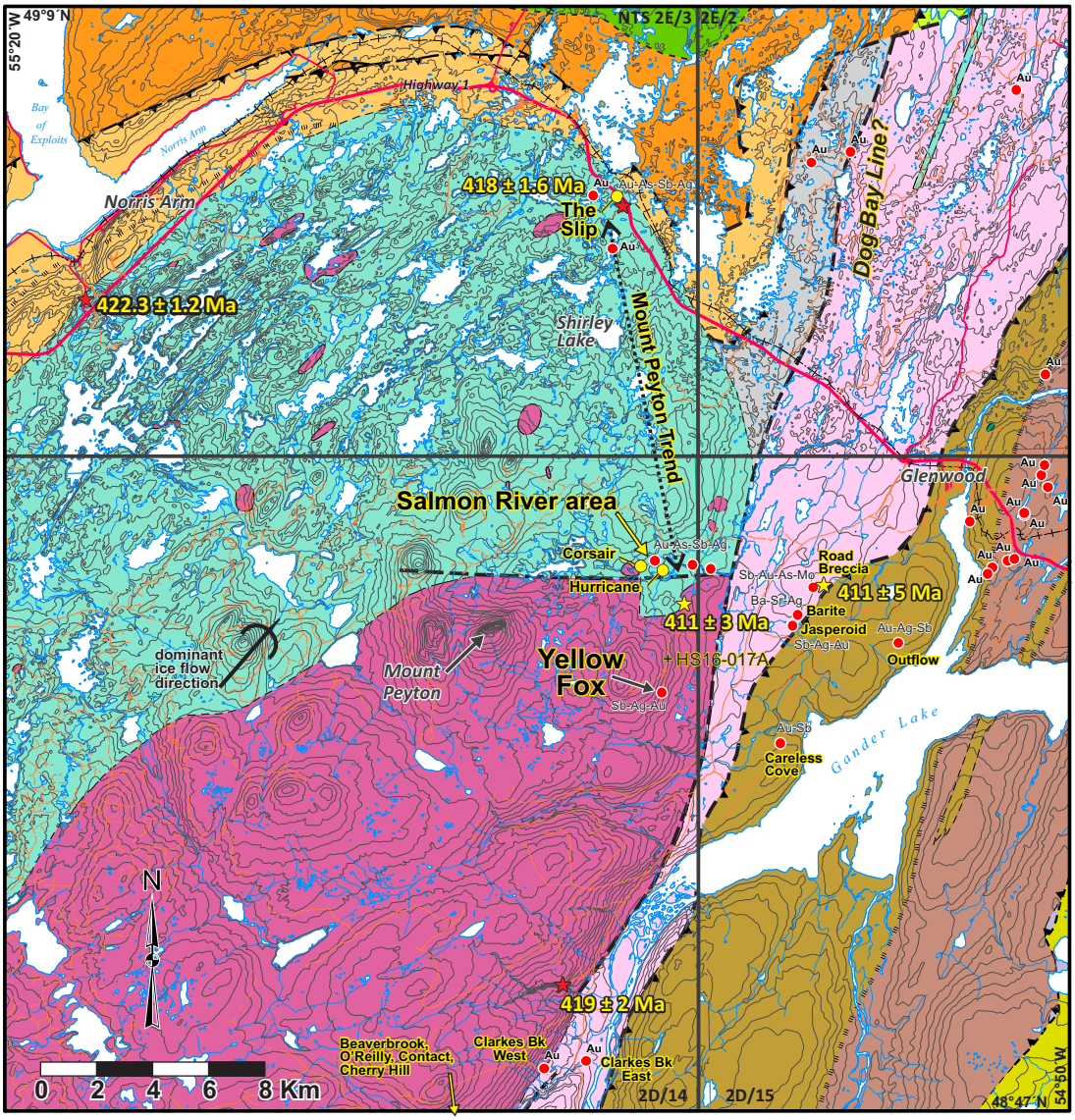

Figure 2. *(Caption on page 2)*

Pollock *et al.*, 2007). The rocks of the Exploits Subzone are largely composed of a collage of Ordovician intra-oceanic arcs, back-arcs and associated marine sedimentary rocks, which in its eastern portion, have demonstrably been structurally emplaced over metasedimentary basement rocks of Ganderia (Colman-Sadd *et al.*, 1990; Vaquero-Valverde *et al.*, 2006). Ordovician volcanic and marine sedimentary rocks of the Exploits Subzone are both conformably and unconformably overlain by the Siluro-Devonian overlap sequences of the Badger, Botwood and Indian Islands groups (Evans *et al.*, 1993; Williams, 1993; Currie, 1993; Williams *et al.*, 1995; O'Brien, 2003). Collectively, these diverse units have been intruded by Late Silurian to Early Devonian intrusive and hypabyssal rocks of the Mount Peyton and Fogo Island intrusive suites (Dickson, 1996; van Staal *et al.*, 2014).

The greater Mount Peyton area (Figures 1 and 2) has been the subject of extensive governmental work, much of which has been summarized by Dickson (1993, 1994, 1996, 2006), O'Driscoll and Wilton (2005), McNicoll *et al.* (2006) and Dickson *et al.* (2007), and the character and styles of mineralization in the region have been documented by Tallman (1991b), Tallman and Evans (1994), Evans (1996), O'Driscoll and Wilton (2005), Squires (2005) and Lake and Wilton (2006). Sandeman *et al.* (2017) provided an updated summary of previous work on the MPIS, examined the age and composition of components of the intrusive suite, and presented new observations on the setting, petrography and structure of the Hurricane and Corsair zones of the Salmon River area and the Slip showing in the Neyles Brook quarry; all of which occur in the granitoid rocks of the MPIS. The relative age, lithostratigraphic and structural geology of the rocks proximal to, and hosting, the Beaver Brook Antimony Mine were discussed in Sandeman *et al.* (2018) who provide the most recent geological summary of the area. Previous investigations in the region pertaining to the age, petrochemistry and contact relationships of the granitoid rocks are briefly reviewed below.

Baird *et al.* (1951) recognized that a large part of north central Newfoundland is underlain by gabbroic and granitic rocks that intrude adjacent sedimentary units. The first 1:250 000-scale map of the region (Williams, 1962) outlined a large gabbro to diorite intrusion cut by monzogranite, outcropping to the south of the community of Norris Arm (Figures 1 and 2). Williams (*op. cit.*) proposed a Devonian age for these intrusive rocks, but stated that 'the relationships of these various rock types are not well known'. The intrusive rocks were included in the regional 1:250 000-scale map of Anderson and Williams (1970).

The earliest geochronological work on the MPIS yielded imprecise K–Ar ages from widely separated localities ranging from 418 ± 21 to 270 ± 52 Ma (Wanless *et al.*, 1967). Subsequently, four granitic (*s.l.*) rocks of the MPIS yielded a Devonian Rb–Sr whole-rock isochron age of 380 ± 30 Ma (Bell *et al.*, 1977). Biotite from the gabbroic part of the MPIS gave a conventional K–Ar date of 410 ± 21 Ma (Williams, 1962; Anderson and Williams, 1970). These early radiometric data were supplemented by more precise ^{40}Ar–^{39}Ar step-heating plateau ages for hornblende and biotite, from a MPIS gabbro sample obtained near Norris Arm that yielded overlapping plateau ages suggesting a 420 ± 8 Ma, latest Silurian age (Reynolds *et al.*, 1981). A reconnaissance petrological study, focused mainly on the northern part of the intrusive complex, outlined that the granitoid rocks comprise a bimodal geochemical assemblage of granite and gabbro (Strong, 1977). Further petrological investigations (Strong and Dupuy, 1982) demonstrated that the intrusive suite comprises gabbro, formed from mantle-derived melts, and granite (*s.l.*) that formed *via* anatexis resulting from introduction of the mafic magma into the crust. The few intermediate compositions noted (Strong and Dupuy, *op. cit.*) were considered to have formed either by magma mixing between the magmatic end-members and/or contamination of the gabbroic magma by the surrounding metasedimentary country rocks. Regional 1:50 000-scale mapping of the Gander Lake map area at that time (Blackwood, 1982) resulted in the introduction of the term Mount Peyton intrusive suite for these diverse plutonic rocks. Using combined magnetic, gravity and lake-sediment geochemical data (Miller and Thakwalakwa, 1992), the MPIS has been shown to comprise an inward-dipping ellipsoidal gabbro to diorite laccolith intruded, and overlain, by a relatively thin mantle of granite.

Much of the subsequent governmental and academic work on the MPIS has been summarized by Dickson (1993, 1994, 1996, 2006) and Dickson *et al.* (2000) and comprised regional geological mapping, lithogeochemical sample collection and interpretation. An updated lithogeochemical database for the MPIS was included in Dickson and Kerr (2007).

The northern margin of the MPIS gabbro–diorite has been demonstrated to have been emplaced into Late Ordovician to Early Silurian Badger Group sedimentary rocks and yielded a marginal hornfels that was metamorphosed at ~810°C and 2.5 kbar (Hynes and Rivers, 2002). The western contact of the MPIS comprises a km-scale-wide zone of migmatitic agmatite consisting of angular, biotite psammite paleosome blocks engulfed by a granodiorite, to locally gabbro neosome that passes westward into sandstone hornfels; the agmatite blocks and hornfels are also interpreted as Badger Group strata (Dickson, 1993; Dickson *et al.*, 2000; O'Brien, 2003).

East of the MPIS, and presumably constituting the most westerly unit lying southeast of the Dog Bay Line, are the Silurian, shallow-marine, locally calcareous and macro-fossil-bearing siltstones and sandstones of the Indian Islands Group (Williams *et al.*, 1993; Currie, 1993, 1995; Dickson, 1996). Along its eastern margin, monzogranite of the MPIS intrudes and generates hornfels in 5- to 20-cm-scale bedded muscovitic sandstone and siltstone of probable Silurian age (Dickson, 1993, 1996; Sandeman *et al.*, 2018). These Silurian rocks are demonstrably imbricated with both Middle Ordovician siltstone and sandstone and Late Ordovician graphitic and pyritic, graptolitic shale (Sandeman *et al.*, *op. cit.*). The most recent field, lithogeochemical and geochronological investigations (Sandeman *et al.*, 2017, 2018) have demonstrated that the MPIS exhibits both intrusive, as well as faulted, contacts with southeastward-lying rocks of the Indian Islands Group, and that most of the gabbroic components of the MPIS were emplaced in the interval *ca.* 425.4 to 421.1 Ma, whereas the granitic parts intruded the gabbro–diorite from *ca.* 419.6 to 416.4 Ma.

PREVIOUS EXPLORATION

Exploration for gold in the Mount Peyton area began in the late 1980s, accompanying an increase in the price of gold bullion. Subsequent to the release of a government regional lake-sediment survey that covered the Mount Peyton area (Davenport and Nolan, 1989), Noranda Exploration Ltd. staked claims and conducted reconnaissance prospecting and regional-till and lake/stream-sediment sampling programs in the northeastern parts of the MPIS (Tallman, 1990). These investigations resulted in the discovery of a number of bedrock gold showings along the Salmon River that yielded up to 25.8 g/t Au and accompanying elevated Ag, Sb and As (Tallman, 1990). In 1990, geophysics, trenching and diamond drilling were completed and led to the discovery of a number of north- and north-northeast-striking, moderately east-dipping mineralized zones including the Hurricane and Corsair prospects (Figure 2; Tallman, 1991a).

Modest exploration for gold in central Newfoundland in the mid-1990s led to Forex Resources' discovery of the Slip showing (Figure 2) in 1993 (Clarke, 1996), hosted by the MPIS and located off the TCH in the Neyles Brook Quarry. Renewed gold exploration in 1999, particularly in the Shirley Lake area (Figure 2; Evans and Dimmell, 2001; Evans *et al.*, 2001), revealed anomalous lake-sediment, soil and bedrock samples defining a north-northwest-trending, 13.5-km-long corridor hosting gold, arsenic and antimony occurrences known as 'the Peyton' or 'the Mount Peyton' trend (Tallman, 1991a; Evans, 1996; Evans and Dimmell, 2001; Evans *et al.*, 2001; Hoffe and Sparkes, 2003; House, 2003, 2005, 2007a, b).

From 2002 to 2007, Rubicon Minerals explored the northeastern parts of the MPIS and completed a regional program including detailed (75-m- and 50-m-line spacing), helicopter-borne aeromagnetic programs, soil-sampling surveys and two diamond drill-holes on the Hurricane prospect (Figure 2; House and McConnell, 2003; Moore and Smith, 2003; House 2007a). Rubicon Minerals also supported a B.Sc. (Hons.) thesis (Hoffe, 2003) encompassing a detailed, multi-element lithogeochemical and geochronological examination of the phases of the MPIS at the Slip showing, results of which are summarized in a mineral-exploration industry assessment report (Hoffe and Sparkes, 2003) and a recent current research report (Sandeman *et al.*, 2017). Further work in the area around the Slip showing (Quinlan, 2009) resulted in the discovery of two additional bedrock and float occurrences, for which fourteen samples returned anomalous gold values ranging from 12 to 12 880 ppb. Those samples consisted of mineralized quartz veins, or quartz vein breccia hosted by gabbro of the MPIS (Quinlan, *op. cit.*).

To the east and southeast, along the margin of the MPIS, many new mineralized zones consisting of epithermal quartz veins, vein breccias and disseminated mineralization in altered wall rock were concurrently discovered and explored (Figure 2; Barbour and Churchill, 1999, 2004; O'Reilly and Churchill, 2004; O'Driscoll and Wilton, 2005; Squires, 2005; House, 2005, 2007a, b; O'Reilly *et al.*, 2008, 2010; Quinlan, 2013). Results outlined northeast-trending zones of veining, silicification and brecciation with disseminated and vein-hosted Au–Ag–As–Sb mineralization at the Mustang and Piper zones (Barbour and Churchill, 2004) as well as epithermal, vuggy and chalcedonic vein- and vein-breccia-related Au ± As ± Ag ± Sb ± Mo mineralization at the O'Reilly showing (O'Reilly *et al.*, 2008, 2010). A number of other discoveries including the Cherry Hill, Clarkes Brook East and Contact showings (Squires, 2005; O'Reilly *et al.*, 2008) all appear to have metal associations similar to those described above. The Yellow Fox showing (Figure 2) was discovered about this time through grass-roots prospecting by Metals Creek Resources in May 2011 (Reid and Myllyaho, 2012). Prospecting yielded a number of grab samples having anomalous metals and yielding a maximum gold assay value of 59.41 ppm Au with coincident elevated silver (15.34 ppm Ag) and weakly anomalous antimony (19 ppm Sb) and copper (531 ppm Cu) (Reid and Myllyaho, 2012). The positive results from prospecting resulted in 2 reconnaissance B-horizon soil-sampling lines; however, soil-sampling results were poor, yielding <5 ppb Au. The company then excavated six east–west-oriented trenches and completed channel sampling in 5 of these trenches. Results were positive, yielding up to 306 ppb Au over 26.82 m, however, there has been no further work on the property and the trenches reclaimed in mid-summer 2017.

GEOLOGY OF THE YELLOW FOX SHOWING

Bedrock exposures near the showing are rare and are confined mainly to ground disturbances associated with forest-access road construction. The showing was exposed during the excavation of 6 east–west-oriented trenches, labelled from north to south Trench 1 through 6 (only 5 are shown in Figure 3). The northern 4 trenches exposed fractured, medium-grained, generally equigranular and locally plagioclase porphyritic monzogranite that is either reddened, or bleached and rusty (Figure 3). The few proximal outcrops of Mount Peyton monzogranite typically lack the pervasive fracturing and the reddening or bleaching (Plate 1A) noted at the Yellow Fox showing (Plate 1B–D). The monzogranite underlying the western margins of the 4 northern trenches is the least altered and exhibits minor reddening and fracturing (Plate 1B); however, the remainder of the exposed monzogranite is variably bleached, fractured and rusty and contains sparse disseminated pyrite. The most intensely altered monzogranite occurs along the central, north–south axis of the trenches and consists of strongly bleached, fractured and rusty, muscovite–pyrite–rutile-altered monzogranite (Plate 1C). At the northernmost Trench 1, the intensely muscovite–pyrite-rutile-altered monzogranite is cut by a 4-cm-wide, north-northeast-trending stibnite–quartz–arsenopyrite vein (Plate 1D).

Examination of the bedrock in the trenches revealed three distinct fracture sets (Plate 2). These include: 1) widely spaced, roughly east–west barren fractures; 2) north–south trending, 5 to 20 cm-spaced fractures in muscovite–pyrite–rutile-altered monzogranite and; 3) sparse, north-northeast-trending, locally stibnite–quartz–arsenopyrite-

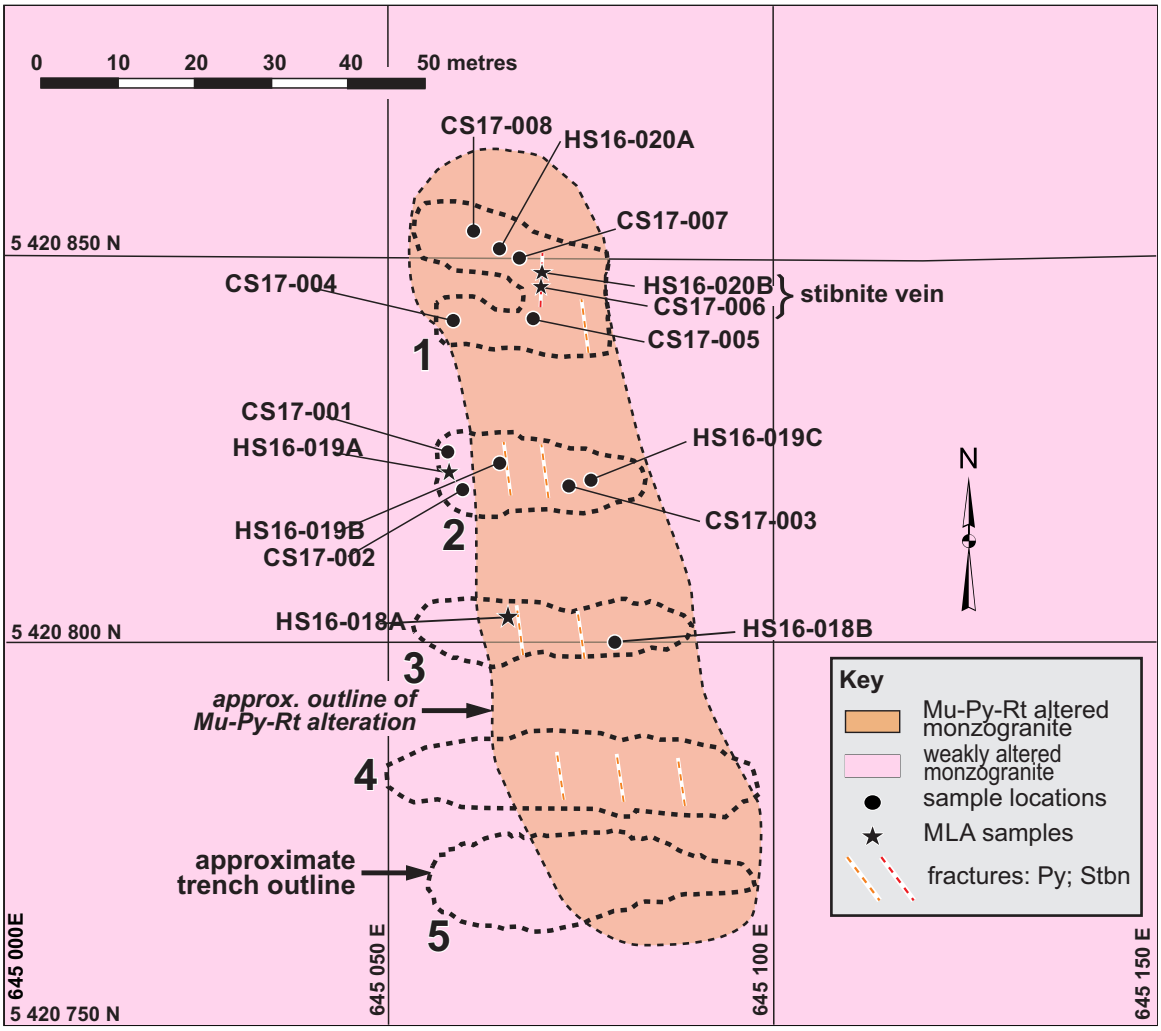

Figure 3. *Geological sketch map of the Yellow Fox showing as determined through examination of the industry trenches (Reid and Myllyaho, 2012). Also shown are sample locations (except HS16-017A;* see *Figure 2), the approximate distribution of alteration and, a few representative, salient fractures.*

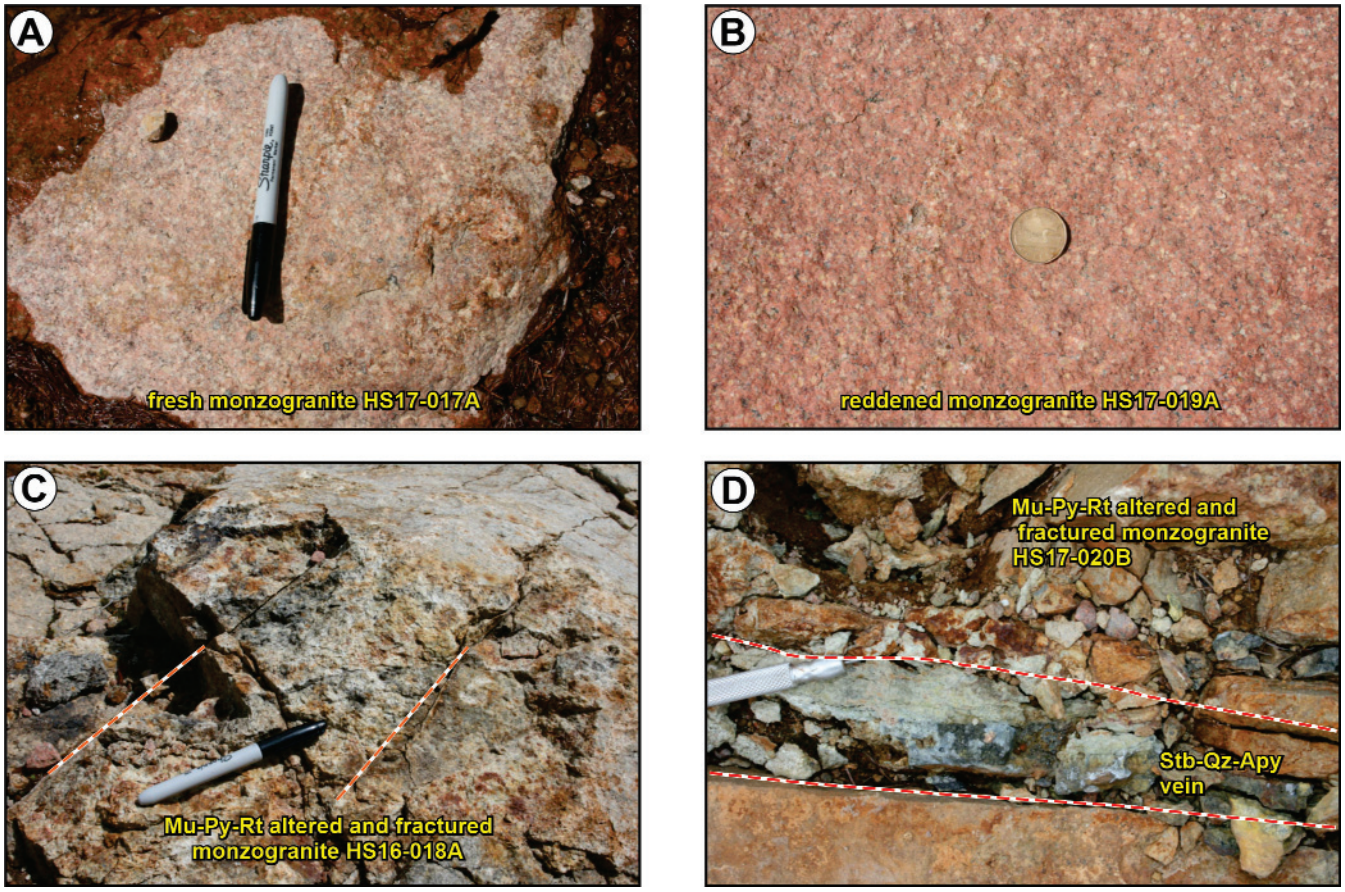

Plate 1. *Representative photographs. A) Relatively fresh, unaltered plagioclase porphyritic monzogranite (sample HS16-017A: UTM's 645117E, 5421989N); B) Reddened, weakly plagioclase porphyritic monzogranite at the western margin of Yellow Fox Trench 2 (Figure 3: sample station HS16-019A: UTM's 654048E, 5420802N); C) Bleached and fractured, muscovite–pyrite– rutile altered monzogranite from Yellow Fox Trench 3 (Figure 3: sample station HS16-018A: UTM's 645081E, 5420793N); D) The ≤4-cm-wide stibnite–quartz–arsenopyrite vein cutting bleached monzogranite at the discovery outcrop in Trench 1 (Figure 3: sample station HS16-020B: UTM's 645069E, 5420827N). Marker and pen magnet in photos point north.*

veined fractures. An equal area stereographic projection of the poles to fractures (Figure 4) indicates that the barren (green) fractures have a mean orientation of 98°/84°S, the muscovite–pyrite–rutile-mineralized fractures (orange) have a mean orientation of 356°/80°E and, the stibnite–quartz–arsenopyrite-veined (red) fractures have a mean orientation of 25°/86°E.

SAMPLING AND ANALYTICAL METHODS

Nineteen bedrock samples were collected from the Yellow Fox trenches and showing area for petrographic and lithogeochemical analysis and include: 4 samples of relatively fresh monzogranite from the peripheries of the industry trenches and one from 1 km north of the showing (including 2 duplicate analyses); 11 samples of altered and fractured, muscovite–pyrite–rutile-altered monzogranite from the trenches and; 3 samples of strongly altered monzogranite cut by a stibnite–quartz–arsenopyrite-bearing vein (Table 1). Of the nineteen samples, three were selected for further detailed petrographic analysis using mineral liberation analysis-scanning electron microscopy (MLA-SEM). These three samples were selected to illustrate the mineralogical changes in the granite in and around the mineralized zone as they span the complete spectrum of fresh or deuterically altered through strongly hydrothermally altered monzogranite marginal to the stibnite vein.

All samples were crushed and processed for standard lithogeochemistry and were analyzed at the Government of Newfoundland and Labrador, Department of Natural Resources Howley Building Laboratory using: Inductively Coupled Plasma-Optical Emission Spectrometry (ICP-OES) for the major elements and selected trace elements including Ag and Inductively Coupled Plasma Mass Spectrometry (ICP-MS) for selected trace elements and the

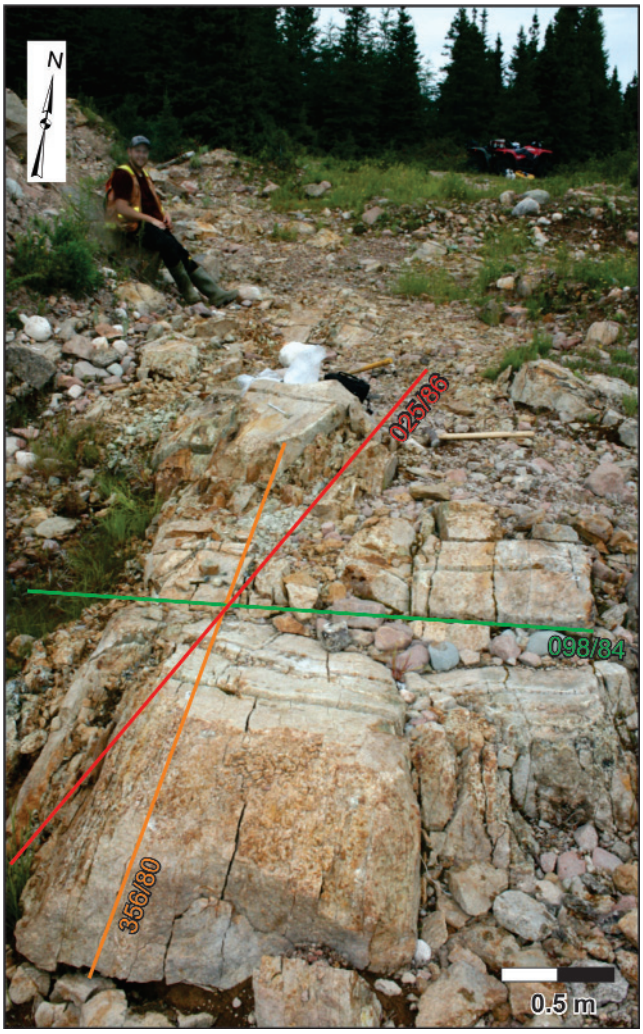

Plate 2. *Photograph looking north, showing the distribution and disposition of barren and mineralized fracture sets at the Yellow Fox showing. Illustrated are the planes of barren fractures (green; 98°/84°E), muscovite–pyrite–rutile-mineralized fractures (Orange; 356°/89°E) and stibnite–quartz–arsenopyrite-veined fractures (Red; 25°/86°E). Note the cut channel samples that parallel to the barren, east–west fracture system.*

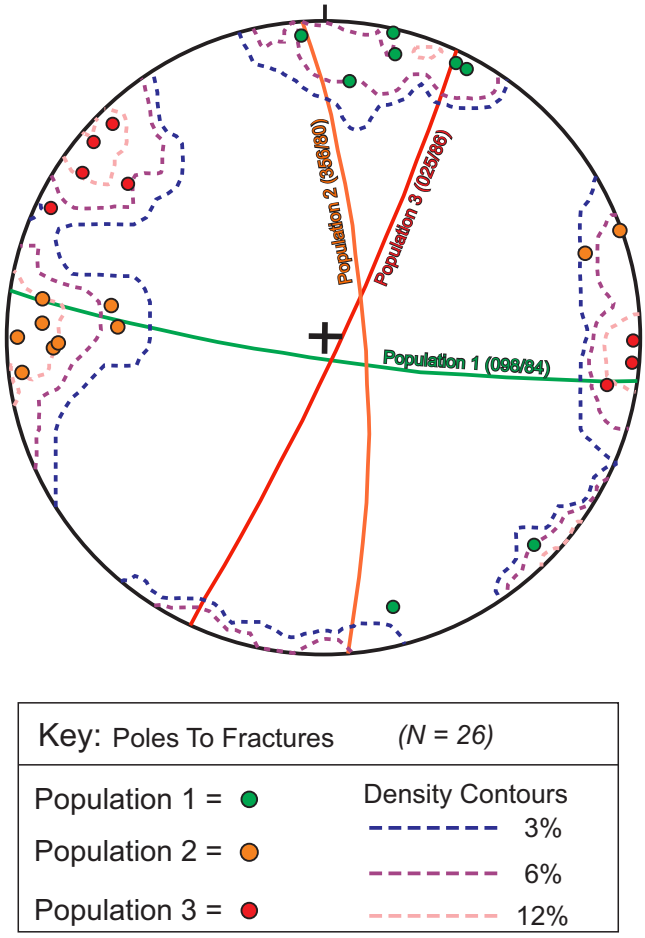

Figure 4. *Lower hemisphere, equal-area plot of poles to barren, muscovite–pyrite–rutile-altered, and stibnite–quartz–arsenopyrite-veined fractures.*

rare-earth elements (REE). Gold, Cd, Bi, As and Sb were determined *via* Instrumental Neutron Activation Analysis (INAA) at Bureau Veritas Laboratories (www.bvlabs.com: formerly Maxxam Analytics) using their standard techniques. Fluorine was analyzed using an ion specific electrode. Complete analytical methods are given in Finch *et al.* (2018) and Sandeman *et al.* (2017) and the data are presented in Table 1. These lithogeochemical data are compared to regional samples of fresh monzogranite from the northern part of the MPIS in order to examine their petrogenesis, and to altered and mineralized rocks of the suite for a comparison of the metal enrichment signatures of the mineralized zone (Tallman, 1991a; Evans, 1996; Evans and Dimmell, 2001; Evans *et al.*, 2001; Hoffe and Sparkes, 2003; House, 2003, 2005, 2007a, b; Dickson and Kerr, 2007; Sandeman *et al.*, 2017). Strongly elevated Sb in the stibnite–quartz–arsenopyrite-veined monzogranite resulted in gamma-ray spectral interference in the INAA data that yielded unresolvable Au in those analyses. Hence, the mineral-exploration fire assay data for gold (Reid and Myllyaho, 2012) are more useful for interpretation.

One representative sample each of reddened monzogranite, bleached muscovite–pyrite–rutile-altered monzogranite and the stibnite–quartz–arsenopyrite-veined monzogranite were selected for qualitative mineral chemical analysis and MLA imaging of thin sections using a FEI MLA 650FEG(2) Scanning Electron Microscope (SEM) at Memorial University of Newfoundland and Labrador Micro Analysis Facility (MUN MAF-IIC). Qualitative analyses were completed with high throughput Energy-dispersive X-ray spectroscopy (EDX) detectors from Bruker (Bruker

Mineral Assay Gun. https://www.mun.ca/creait/). The purpose of this SEM work was to map the electron energy spectra of the thin section in order to identify all minerals; in particular, fine-grained alteration phases, and to visually illustrate diagnostic mineral textures.

A cut representative piece of each of the 19 rock samples were analyzed using visible/infrared reflectance spectrometric (VIRS) analysis collected on and exported from a TerraSpec® Pro spectrometer. Spectral and mineral identification of the VIRS data were determined using the TSG™ Pro software. A summary of this method and its applications at the Geological Survey of Newfoundland and Labrador are presented in Kerr *et al.* (2011). Each sample was scanned at least twice in order to test analytical reproducibility. Within the dataset (Table 2), an estimate of the relative proportions of the two dominant mineral phases within each sample are provided (wt. % mineral 1 and wt. % mineral 2), along with a corresponding error related to the overall 'fit' of the sample spectra relative to reference spectra in the TSG™ Pro spectral database (Error_sTSAS). The lower the error value, the better the match with the reference spectra. Because of the nature of the alteration, absorption features in the short-wavelength-infrared region (~1300–2500 nm) characteristic of the white mica minerals are the main topic of interest. Table 2 also provides the calculated depth of wavelength troughs for three characteristic (1400, 1900 and 2200 nm) absorption features of white micas along with the position of the 2200 nm absorption feature and estimates of the illite spectral maturity (ISM (H_2O)) for the samples.

ANALYTICAL RESULTS

VIRS ANALYSIS

Whereas all samples have muscovite as a significant hydrous mineral, six analyses from three specific samples contain additional hydrous minerals. The representative, regional monzogranite sample HS17-017A contains muscovite with chlorite and siderite. The marginal, weakly altered and reddened monzogranite HS16-019A is characterized by a phengitic white mica. The stibnite–quartz–arsenopyrite-veined monzogranite sample HS17-020B yielded two analyses with only muscovite and two with both muscovite and chlorite (Table 2). A plot of illite spectral maturity (Doublier *et al.*, 2010) or ISM(H_2O) *vs.* the white mica ~2200 nm spectral trough position (Duke, 1994) outlines the distinction between the muscovite only, *vs.* muscovite–chlorite- or phengite-bearing samples (Figure 5A). On this diagram, the six differing analyses with spectral trough positions at >2205 nm have lower spectral maturity, corresponding lower crystallinity, and hence plot to the right of the remainder of the samples. Similarly, the six distinct analyses have relatively small ~2200 *vs.* ~1900 nm troughs, corresponding with low ISM (H_2O), and fall on a distinct array from the remainder of the analyses (Figure 5B). These observations indicate that the VIRS analyses of the least altered monzogranite sampled less crystalline white mica that was formed at lower temperatures than those in the muscovite only samples. The two analyses of the stibnite–quartz–arsenopyrite-veined sample (HS16-020B), located off the main trend, contain spectral signatures that are dominated by broad water features coupled with weak 2200 nm absorption troughs. Such analyses may result from spectral interference from the vein quartz and chlorite present within the sample.

PETROGRAPHY AND MLA DATA

On the basis of field, VIRS and petrographic observations, the samples are grouped into: 1) regional, background, locally deuterically altered fresh monzogranite; 2) weakly hydrothermally altered monzogranite distal (>25 m) from the central axis of the Yellow Fox fracture and vein systems (HS16-019A); 3) muscovite–pyrite–rutile-altered monzogranite lying within the fractured and veined area (HS16-018A) and; 4) stibnite–quartz–arsenopyrite-veined monzogranite at the core of the fracture systems (HS16-020B). All sample locations (Table 1; Figures 2 and 3) are recorded in NAD27 datum and UTM zone 21. Below we discuss the petrographic characteristics of the monzogranite with respect to the collective petrography of all samples, but in particular, with reference to the three samples chosen for MLA analysis.

Regional, Fresh Monzogranite (*e.g.*, HS16-017A)

Sample HS16-017A is a representative plagioclase porphyritic, fine- to medium-grained, granophyric-textured, hornblende–biotite monzogranite obtained from a small borrow pit on the north side of the Yellow Fox access road, ~1 km north of the showing (Figure 2). Plagioclase phenocrysts are variably saussuritized, although lamellar twinning is locally preserved (Plate 3A, B). Mafic mineral phases are sparse, forming small clots in what are interpreted as miarolitic cavities between the quartz and feldspars that include: variably chloritized, subhedral, bladed biotite, subhedral dark green hornblende with sparse anhedral grains of intergrown magnetite and ilmenite, and minor euhedral zircon and subhedral commonly accicular apatite (Plate 3B).

Weakly Altered Reddened Monzogranite (*e.g.*, HS16-019A)

Sample HS16-019A is a representative, incipiently altered, medium-grained, plagioclase porphyritic, granophyric-textured biotite–hornblende monzogranite of the MPIS that was collected from the west end of Trench 2

Table 1. Lithogeochemical data for samples from the Yellow Fox showing. Negative numbers indicate detection limits. Large negative numbers for INAA data further indiate significant spectral interference

Sample	CS17-001	CS17-002	CS17-003	CS17-004	CS17-005	CS17-006	CS17-007	CS17-008	HS16-017A
Lab Number	8941276	8941277	8941278	8941279	8941339	8941281	8941338	8941282	8941124
rock-type	Mu-Py-Rt altered mzgn	Mu-Py-Rt altered mzgn	Mu-Py-Rt altered mzgn	Stbn-Qtz-Apy-veined mzgn	Stbn-Qtz-Apy-veined mzgn	Mu-Py-Rt altered mzgn	Mu-Py-Rt altered mzgn	Mu-Py-Rt altered mzgn	Fresh mzgn
UTM_East	645147	645143	645151	645151	645155	645151	645155	645151	645117
UTM_North	5421026	5421015	5421014	5421014	5421050	5421014	5421050	5421014	5421989
zone	21	21	21	21	21	21	21	21	21
datum	NAD 27	NAD 27	NAD 27	NAD 27	NAD 27	NAD 27	NAD 27	NAD 27	NAD 27
Mg#	12.55	16.05	18.56	3.05	4.00	14.54	19.06	13.98	20.58
SiO_2 (wt.%)	78.20	78.41	78.35	61.59	67.94	77.48	76.14	78.11	73.60
Al_2O_3	11.60	11.85	12.27	8.40	9.87	12.08	12.78	12.35	12.71
$Fe_2O_3^T$	2.61	2.16	1.85	7.31	6.34	2.17	2.34	2.13	2.35
Fe_2O_3	1.21	0.71	NA	0.65	1.93	0.70	0.60	0.85	0.68
FeO	1.26	1.31	NA	5.99	3.97	1.32	1.57	1.15	1.50
MgO	0.19	0.21	0.21	0.12	0.13	0.19	0.28	0.17	0.31
CaO	0.04	0.06	0.05	0.03	0.03	0.03	0.05	0.04	0.13
Na_2O	0.07	0.07	0.05	0.04	0.05	0.06	0.04	0.06	3.02
K_2O	3.63	3.67	3.59	2.56	3.07	3.82	3.58	3.82	4.70
TiO_2	0.214	0.209	0.231	0.160	0.177	0.216	0.240	0.174	0.228
MnO	0.055	0.026	0.013	0.030	0.027	0.025	0.085	0.038	0.020
P_2O_5	0.016	0.018	0.020	0.014	0.014	0.016	0.023	0.019	0.024
LOI	1.93	2.39	2.67	10.86	7.93	2.28	2.69	2.18	1.67
Total	98.55	99.08	99.31	91.11	95.59	98.36	98.23	99.10	98.76
F (ppm)	491	500	547	379	435	570	547	552	381
Cr	6	7	5	4	14	6	5	5	6
Zr	177	200	223	168	173	230	283	152	231
Ba	498	387	140	304	389	396	124	384	402
Be	1.8	1.8	2.7	1.9	2.0	2.0	2.8	2.1	2.5
Sc	7.2	7.3	7.5	4.9	6.1	7.3	8.4	6.7	8.4
Ag	0.1	0.2	0.2	5.1	1.2	1.3	-0.1	0.2	-0.1
As	75	2463	29	39700	33000	3815	189	1655	6
Cd	0.2	2.2	0.1	206.2	123.2	4.1	0.3	0.9	-0.1
Co	-5	-5	-5	-5	-5	-5	-5	-5	2
Cu	22	20	18	480	140	63	10	16	3
Li	11.9	13.7	34.1	12.8	11.7	11.1	35.1	10.8	11.9
Mn	428	200	98	236	206	194	656	291	158
Ni	4	3	3	8	7	3	4	3	5
Pb	346	262	47	19800	8642	484	63	619	5
Rb	108	111	137	89	115	126	154	125	176
V	8	8	8	6	6	8	9	5	7
Zn	85	286	87	10600	4005	424	29	62	22
Ga	17	18	17	13	15	18	19	20	21
Ge	1.5	1.6	1.4	1.3	-1.0	1.7	1.5	1.1	6.3
Sr	3	4	101	9	6	3	5	2	27
Y	48	58	53	33	38	51	54	60	87
Nb	9	9	11	8	9	9	10	9	11
Mo	4.6	3.4	-2.0	2.2	-2.0	2.3	3.4	-2.0	-2.0
Sn	14	20	8	14	14	16	4	21	4
Cs	1.5	1.5	2.1	1.5	1.6	1.7	1.9	1.7	1.8
La	36.82	34.97	39.07	33.39	34.87	38.44	55.49	47.27	86.29
Ce	82.06	81.10	90.41	63.88	68.99	86.42	107.30	99.21	115.67
Pr	9.44	9.35	10.67	8.54	8.70	10.34	12.73	11.95	22.18
Nd	35.70	36.85	41.43	31.99	34.31	38.69	46.83	45.53	84.98
Sm	7.95	8.62	9.12	7.33	7.67	8.25	10.34	9.75	17.68
Eu	0.77	1.06	0.86	0.54	0.65	0.67	1.02	1.01	1.57
Gd	8.48	9.73	9.66	6.42	7.17	9.10	10.17	10.11	16.71
Tb	1.45	1.66	1.65	1.04	1.19	1.53	1.72	1.79	2.52
Dy	8.52	10.53	10.00	6.14	6.98	9.54	10.37	11.02	14.87
Ho	1.67	2.12	2.06	1.29	1.45	1.92	2.03	2.14	2.90
Er	5.13	6.57	6.14	3.76	4.25	5.90	6.28	6.67	8.77
Tm	0.77	0.97	0.91	0.57	0.63	0.83	0.92	1.02	1.13
Yb	5.11	6.28	5.84	3.70	4.50	5.58	6.13	6.55	8.03
Lu	0.75	0.96	0.96	0.56	0.68	0.97	0.99	1.02	1.21
Hf	5.58	6.23	7.02	4.53	5.39	6.91	8.46	5.06	7.42
Ta	-1.0	-1.0	-1.0	3.0	-1.0	-1.0	1.5	-1.0	0.7
W	1.7	2.8	-1.0	3.0	5.5	3.6	1.5	3.1	-1.0
Tl	-0.1	-0.1	-0.1	-0.1	-0.1	-0.1	-0.1	-0.1	-0.5
Bi	-0.5	-0.5	-0.5	-0.5	-0.5	-0.5	-0.5	-0.5	-0.5
Th	16.68	17.74	18.72	12.67	13.66	18.32	19.00	20.64	18.84
U	4.21	4.43	4.16	5.92	3.52	3.60	4.73	5.08	3.84
Sb	208	98.6	35.2	40700	13300	290	40.2	524	1.6
Br	-1	-1	-1	-320	-87	-1	-1	-1	-1
Au (ppb)	38	692	5	-800	-277	294	153	317	-1
Se	-2	-2	-1	-130	-37	-4	-1	-9	-1

Table 1. Continued

HS16-018A	HS16-018B	HS16-019A	HS16-019A DUP	HS16-019B	HS16-019C	HS16-020A	HS16-020B	HS17-019	HS17-020B
8941174	8941175	8941125	8941130	8941176	8941177	8941178	8941179	8941302	8941304
Mu-Py-Rt	Mu-Py-Rt			Mu-Py-Rt	Mu-Py-Rt	Mu-Py-Rt	Stbn-Qtz-Apy-		
altered mzgn	altered mzng	Reddened mzgn	Reddened mzgn	altered mzgn	altered mzgn	altered mzgn	veined mzgn	Fresh mzgn	Fresh mzgn
645081	645092	654048	654048	645062	645086	645066	645069	639502	645980
5420793	5420789	5420802	5420802	5420807	5420804	5420836	5420827	5408229	5424008
21	21	21	21	21	21	21	21	21	21
NAD 27	NAD 27	NAD 27	NAD 27	NAD 27	NAD 27	NAD 27	NAD 27	NAD 27	NAD 27
22.50	13.94	15.24	16.25	14.20	14.75	15.71	1.21	14.21	15.78
78.39	75.80	73.45	73.97	77.04	74.53	76.41	48.66	73.00	73.15
11.92	12.18	12.70	12.56	12.28	12.94	13.70	5.87	12.76	12.18
1.84	3.48	1.91	1.89	2.46	2.98	2.42	15.37	2.73	2.31
0.15	NA	0.72	0.68	0.31	1.03	0.18	4.86	1.73	0.81
1.52	NA	1.07	1.09	1.93	1.76	2.01	9.46	0.90	1.35
0.27	0.28	0.17	0.19	0.21	0.26	0.23	0.10	0.23	0.22
0.05	0.07	0.18	0.20	0.20	0.04	0.06	0.04	0.36	0.50
0.05	0.31	3.01	2.97	0.06	0.16	0.17	0.05	3.38	3.21
3.44	3.70	4.99	4.91	3.67	4.82	3.70	1.80	4.90	4.81
0.218	0.227	0.222	0.218	0.229	0.231	0.252	0.115	0.304	0.232
0.013	0.022	0.042	0.041	0.101	0.017	0.022	0.037	0.029	0.029
0.018	0.026	0.026	0.026	0.017	0.029	0.027	0.012	0.043	0.025
2.17	2.87	1.34	1.27	2.01	2.36	2.65	21.34	1.96	1.47
98.38	98.97	98.04	98.25	98.26	98.36	99.63	93.39	99.70	98.12
738	963	380	401	832	866	596	280	81	137
6	-1	4	5	4	4	9	3	8	6
217	219	224	216	245	250	223	104	300	216
121	349	446	439	391	360	105	192	512	541
2.1	3.1	2.8	2.7	2.0	2.9	3.2	1.7	1.9	2.1
7.7	9.4	8.6	8.7	8.7	9.1	9.2	3.9	7.5	7.9
0.3	-0.1	-0.1	-0.1	-0.1	0.3	0.1	2.5	-0.1	-0.1
98	17	4	4	31	15	124	129000	4	3
0.6	0.1	-0.1	-0.1	0.5	0.1	0.5	717.5	-0.1	-0.1
-1	2	2	2	3	1	1	7	-5	-5
12	16	2	3	18	12	7	135	8	3
27.1	23.8	12.8	12.9	10.8	20.6	27.9	11.6	32.2	14.7
112	169	336	336	817	136	181	181	226	226
4	5	4	4	5	4	4	14	4	4
33	50	4	4	529	57	132	29970	16	11
130	159	209	210	110	176	142	60	203	170
8	8	8	7	8	8	8	4	10	9
86	61	22	22	110	52	66	97	58	31
16	19	18	18	17	18	20	9	17	16
3.3	3.2	3.7	4.5	4.5	3.8	5.0	4.4	-1.0	1.3
5	19	31	29	4	32	6	5	31	49
44	65	59	60	66	62	69	36	52	35
13	11	10	9	13	13	15	8	13	13
2.7	4.2	2.0	-2.0	2.9	3.6	3.3	2.1	-2.0	-2.0
5	8	5	5	14	9	5	14	7	4
2.1	0.7	2.5	2.7	1.5	2.6	3.1	1.2	6.2	4.4
40.64	57.20	48.97	46.67	57.65	51.86	66.98	28.93	34.70	24.87
89.68	118.26	101.17	97.56	109.76	113.16	140.46	55.78	77.70	56.61
10.11	13.77	12.69	12.97	14.90	12.12	16.02	7.07	9.38	6.63
37.42	51.02	48.38	50.86	57.08	44.86	59.57	25.96	35.49	25.10
7.94	10.11	10.56	11.23	13.49	8.97	12.52	5.59	8.25	6.26
0.76	0.87	1.12	1.14	1.71	0.72	1.16	0.44	0.96	0.87
8.41	10.68	10.07	10.62	13.84	9.15	12.27	6.07	8.32	6.16
1.40	1.93	1.71	1.80	2.18	1.60	2.03	0.98	1.44	1.08
8.30	11.88	10.69	11.27	12.52	10.60	12.52	6.42	9.19	6.78
1.66	2.44	2.08	2.19	2.54	2.18	2.50	1.31	1.91	1.42
4.92	7.46	6.32	6.89	7.40	6.71	7.59	4.06	5.93	4.23
0.73	1.11	0.87	0.95	1.07	0.96	1.08	0.57	0.86	0.64
4.60	7.12	6.07	6.56	6.97	6.54	6.89	3.69	5.73	4.44
0.75	1.17	0.88	1.00	1.07	0.96	1.08	0.58	0.95	0.67
6.92	7.09	6.80	7.24	7.83	7.86	7.11	3.14	7.89	6.40
1.9	1.4	-0.5	-0.5	1.9	2.0	1.9	2.9	2.5	2.5
2.2	1.5	-1.0	-1.0	3.0	2.4	3.9	3.9	3.3	-1.0
-0.5	-0.5	-0.5	-0.5	-0.5	-0.5	-0.5	-0.5	-0.1	-0.1
-0.5	-0.5	-0.5	-0.5	-0.5	-0.5	-0.5	-0.5	-0.5	-0.5
17.51	17.18	18.28	18.19	18.41	19.47	19.83	8.84	17.07	17.15
3.63	4.55	4.29	4.75	4.61	4.61	4.91	6.27	4.79	4.41
46.7	40.8	6.1	6.6	30.6	38.1	48.7	22800	0.9	1.3
-1	-1	-1	-1	-1	-1	-1	-80	-1	-1
24	6	-1	-1	8	5	87	-510	-1	-1
-1	-1	-1	-1	-1	-1	-1	-160	-1	-1

Table 2. VIRS data for samples from the Yellow Fox showing. Illite spectral maturity [ISM(H_2O)] is the value of the depth of the 2200 nm trough/depth of the 1900 nm trough (Doublier *et al.*, 2010)

Sample	Rock-type	Identified mineral 1	Wt. % mineral 1	Identified mineral 2	Wt. % mineral 2	Error_ sTSAS	Depth_ 1400nm	Depth_ 1900nm	Depth_ 2200nm	WhitMica _Comp	ISM_H2O
CS17-001	fractured Mu-Py-Rt-altered monzogranite	Muscovite	1	NULL	NULL	102.61	0.325	0.167	0.449	2202.86	2.686
CS17-001-2	fractured Mu-Py-Rt-altered monzogranite	Muscovite	1	NULL	NULL	91.90	0.414	0.229	0.480	2203.27	2.093
CS17-002	fractured Mu-Py-Rt-altered monzogranite	Muscovite	1	NULL	NULL	91.35	0.568	0.550	0.529	2201.84	0.961
CS17-002-2	fractured Mu-Py-Rt-altered monzogranite	Muscovite	1	NULL	NULL	73.03	0.408	0.351	0.418	2202.71	1.192
CS17-003	fractured Mu-Py-Rt-altered monzogranite	Muscovite	1	NULL	NULL	197.32	0.466	0.339	0.471	2198.08	1.390
CS17-003-2	fractured Mu-Py-Rt-altered monzogranite	Muscovite	1	NULL	NULL	149.91	0.437	0.271	0.470	2199.92	1.732
CS17-004	Stbn-Qtz-Apy-veined monzogranite	Muscovite	1	NULL	NULL	85.84	0.466	0.316	0.505	2202.61	1.598
CS17-004-2	Stbn-Qtz-Apy-veined monzogranite	Muscovite	1	NULL	NULL	99.85	0.445	0.242	0.501	2202.87	2.071
CS17-006	fractured Mu-Py-Rt-altered monzogranite	Muscovite	1	NULL	NULL	71.19	0.468	0.435	0.441	2203.85	1.014
CS17-006-2	fractured Mu-Py-Rt-altered monzogranite	Muscovite	1	NULL	NULL	87.11	0.400	0.335	0.425	2204.34	1.268
CS17-007	fractured Mu-Py-Rt-altered monzogranite	Muscovite	1	NULL	NULL	217.59	0.482	0.197	0.520	2198.63	2.636
CS17-007-2	fractured Mu-Py-Rt-altered monzogranite	Muscovite	1	NULL	NULL	177.53	0.346	0.182	0.473	2199.69	2.593
CS17-008	fractured Mu-Py-Rt-altered monzogranite	Muscovite	1	NULL	NULL	95.36	0.459	0.245	0.506	2201.90	2.070
CS17-008-2	fractured Mu-Py-Rt-altered monzogranite	Muscovite	1	NULL	NULL	92.78	0.450	0.207	0.514	2202.75	2.487
HS16-017A	fresh monzogranite	Muscovite	0.585	Chlorite-Fe	0.415	104.30	0.133	0.183	0.132	2207.96	0.719
HS16-017A-2	fresh monzogranite	Muscovite	0.701	Siderite	0.299	106.88	0.072	0.181	0.115	2208.56	0.638
HS16-018A	fractured Mu-Py-Rt-altered monzogranite	Muscovite	1	NULL	NULL	139.41	0.467	0.152	0.525	2200.18	3.460
HS16-018A-2	fractured Mu-Py-Rt-altered monzogranite	Muscovite	1	NULL	NULL	129.78	0.437	0.137	0.471	2201.09	3.429
HS16-018B	fractured Mu-Py-Rt-altered monzogranite	Muscovite	1	NULL	NULL	149.62	0.369	0.236	0.426	2199.51	1.804
HS16-018B-2	fractured Mu-Py-Rt-altered monzogranite	Muscovite	1	NULL	NULL	114.00	0.368	0.177	0.431	2200.77	2.443
HS16-019A	reddened monzogranite	Phengite	1	NULL	NULL	175.99	0.108	0.124	0.158	2208.84	1.275
HS16-019A-2	reddened monzogranite	Phengite	1	NULL	NULL	174.95	0.120	0.122	0.178	2209.40	1.463
HS16-019B	fractured Mu-Py-Rt-altered monzogranite	Muscovite	1	NULL	NULL	100.89	0.414	0.143	0.486	2203.56	3.386
HS16-019B-2	fractured Mu-Py-Rt-altered monzogranite	Muscovite	1	NULL	NULL	97.18	0.409	0.123	0.486	2203.69	3.933
HS16-019C	fractured Mu-Py-Rt-altered monzogranite	Muscovite	1	NULL	NULL	129.01	0.499	0.155	0.533	2202.67	3.452
HS16-019C-2	fractured Mu-Py-Rt-altered monzogranite	Muscovite	1	NULL	NULL	114.60	0.493	0.168	0.536	2202.75	3.185
HS16-020A	fractured Mu-Py-Rt-altered monzogranite	Muscovite	1	NULL	NULL	174.48	0.402	0.176	0.451	2198.83	2.567
HS16-020A-2	fractured Mu-Py-Rt-altered monzogranite	Muscovite	1	NULL	NULL	175.49	0.455	0.194	0.495	2199.26	2.555
HS16-020B	Stbn-Qtz-Apy-veined monzogranite	Muscovite	1	NULL	NULL	79.51	0.355	0.199	0.394	2202.48	1.986
HS16-020B-2	Stbn-Qtz-Apy-veined monzogranite	Muscovite	1	NULL	NULL	90.66	0.386	0.223	0.422	2202.59	1.889
HS16-020B-3	Stbn-Qtz-Apy-veined monzogranite	Muscovite	0.539	Chlorite-Fe	0.461	112.10	0.137	0.152	0.110	2205.77	0.727
HS16-020B-4	Stbn-Qtz-Apy-veined monzogranite	Muscovite	0.548	Chlorite-Fe	0.452	123.82	0.123	0.157	0.123	2206.94	0.785

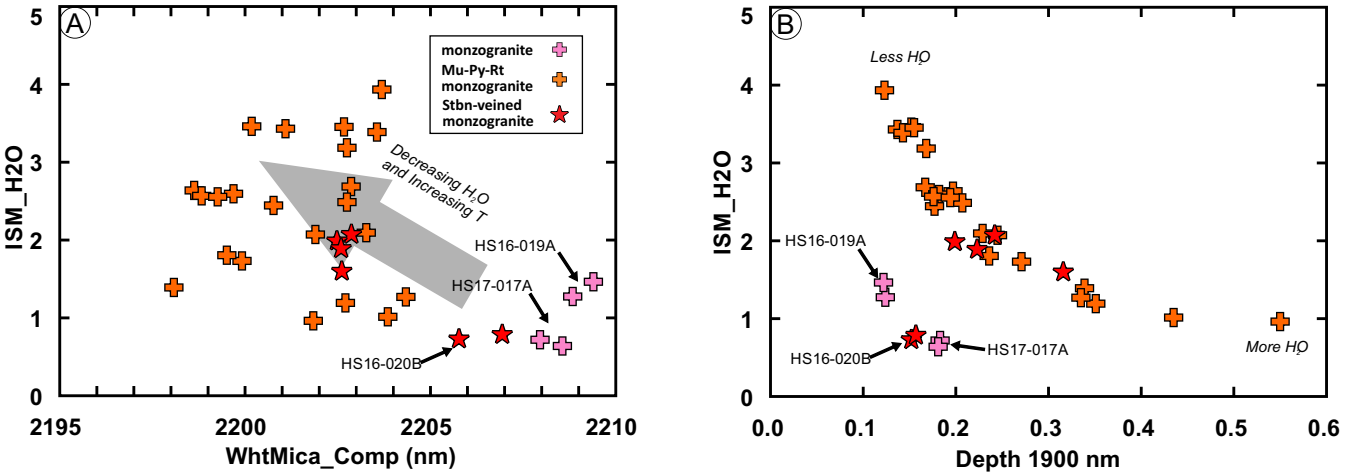

Figure 5. *VIRS data for the Yellow Fox showing. A) Illite spectral maturity (ISM) H_2O* vs. *white mica composition (Al-OH); B) ISM H_2O* vs. *the depth of the 1900 nm absorption trough. ISM (H_2O) corresponds to the depth of the 2200 nm trough/1900 nm trough (Doublier* et al.*, 2010).*

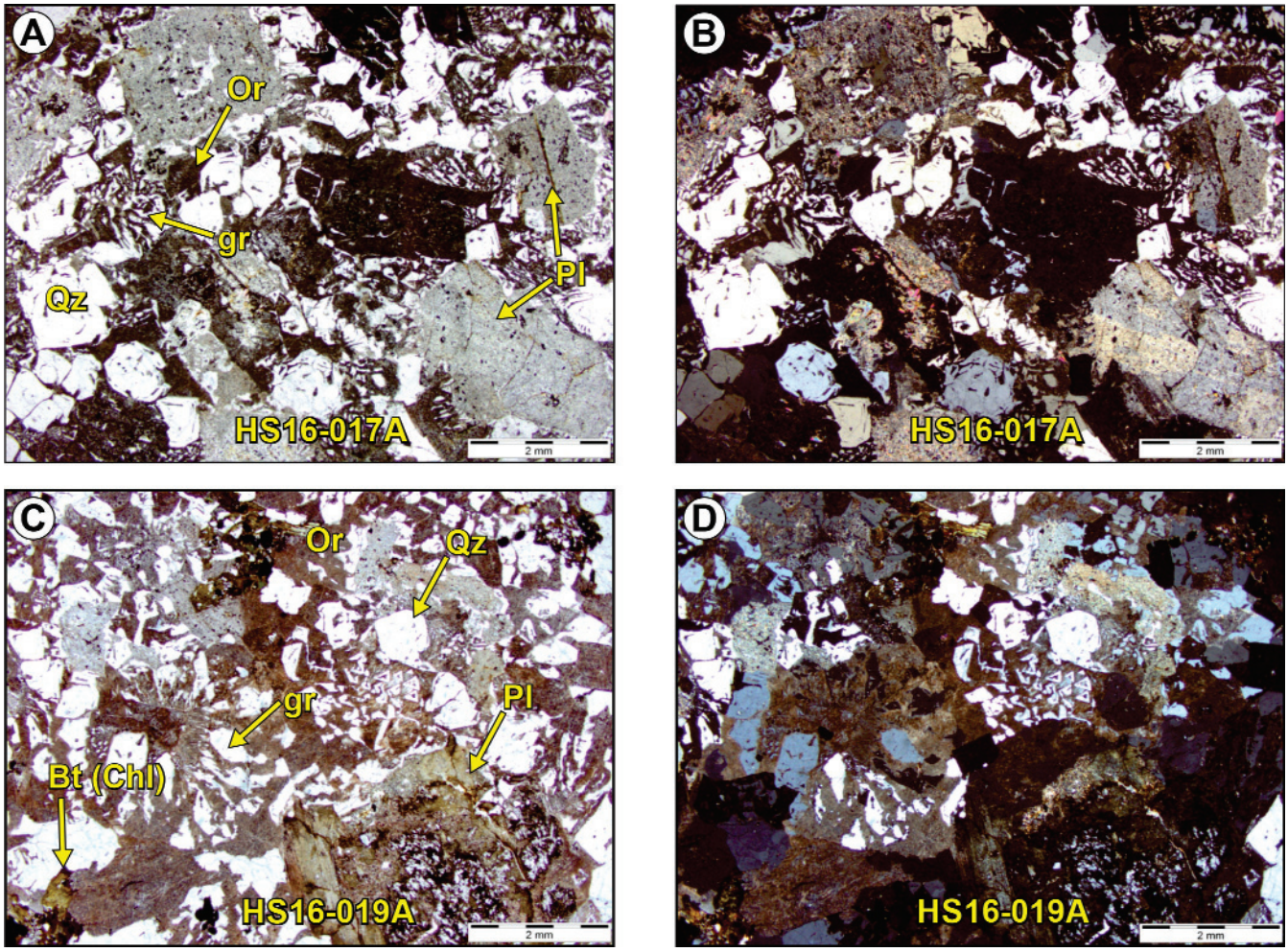

Plate 3. *Representative photomicrographs. A) Fresh, regional monzogranite sample HS16-017A under plane-polarized light (ppl); B) Same field of view of monzogranite sample HS16-017A under crossed nicols; C) Weakly altered, reddened monzogranite sample HS16-019A under ppl; D) Same field of view of monzogranite sample HS16-019A under crossed nicols. Key: Qz–quartz; Pl–Plagioclase; Or–orthoclase; Bt (Chl)–chloritized biotite; gr–granophyric texture.*

(Figure 3; Plate 3C). The rock is reddened, and plagioclase crystals are a pale yellow-green. Plagioclase grains locally appear to preserve oscillatory zoning, which is represented by inner zones preferentially enriched in a fine-grained intergrowth of albite–quartz–muscovite, and outer zones characterized by muscovite alone (Figure 6; Plate 3C, D). Ferromagnesian silicates (biotite and hornblende) occur as inter-grown clots, and are variably altered to chlorite + muscovite + rutile + goethite with common euhedral cubic zircon. The rock consists of 20.3 volume %, subhedral, variably sericitized and saussuritized plagioclase phenocrysts (≤4 mm) and 37.9 % anhedral quartz grains that commonly form granophyric and locally myrmekitic intergrowths with alkali feldspar (21.8%), which constitutes much of the reminder of the rock (Plate 3D; Figure 6). A proportion of the plagioclase, likely more calcic end-members, as well as orthoclase forming the granophyric texture, are variably replaced by muscovite (13.8%), albite and chlorite (2.0%). White mica alteration is minimal in comparison to samples more proximal to the fracture system. Accessory phases include euhedral zircon, subhedral apatite and less common anhedral monazite and xenotime (Figure 6)

Bleached, Fractured Pyritic Monzogranite (*e.g.*, HS16-018A)

Sample HS16-018A represents an altered, fractured monzogranite of the MPIS obtained from Trench 3, approximately 12 m west of the axis of the central, fractured and pyritic zone (Figure 3). This sample is an intensely muscovite-altered, medium-grained, plagioclase-phyric, granophyric-textured monzogranite with essentially all primary feldspar phases (plagioclase and orthoclase) entirely replaced by muscovite. Figure 7 illustrates that a number of the muscovite-dominant patches have partial rectangular outlines reflecting pseudomorphed plagioclase phenocrysts and, that what was primary granophyric texture is now intergrowths of muscovite lamellae in quartz (Plate 4A, B).

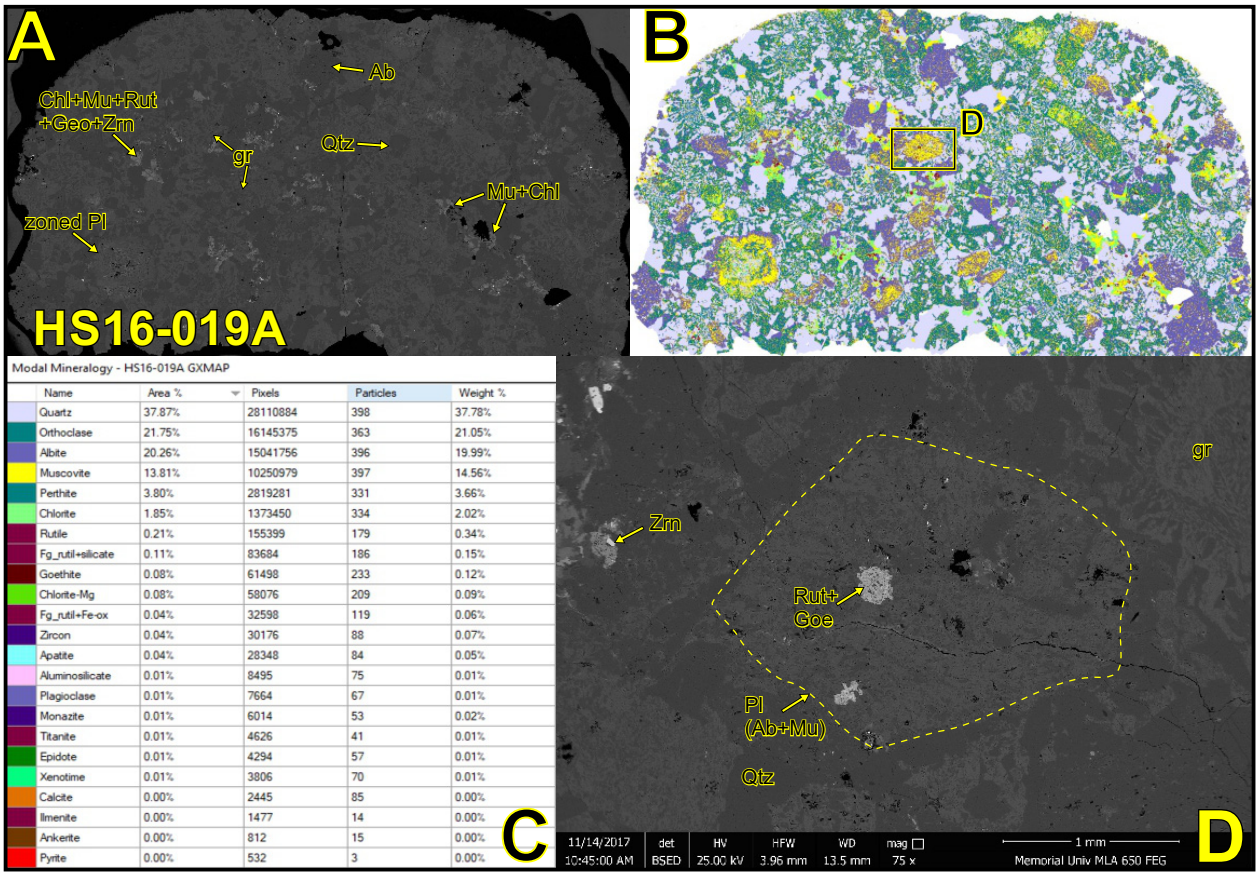

Figure 6. *Electron microprobe MLA imagery for sample HS16-019A composed of reddened, weakly altered monzogranite from the western margin of Yellow Fox Trench 2. A) Backscattered electron (BSE) image of the thin section; B) MLA false colour image of the mineralogy of the thin section, showing the locations of image D; C) Coloured legend for B; D) BSE image of a sericite-altered plagioclase phenocryst with a rutile and goethite inclusion, surrounded by granophyric intergrowths of orthoclase and quartz. Key: Qtz–quartz; Chl–chlorite; Mu–muscovite; Apy–arsenopyrite; Pl–plagioclase; Ab–albite; Goe–goethite; Or–orthoclase; Rut–rutile; gr–granophyric texture; Zrn–zircon.*

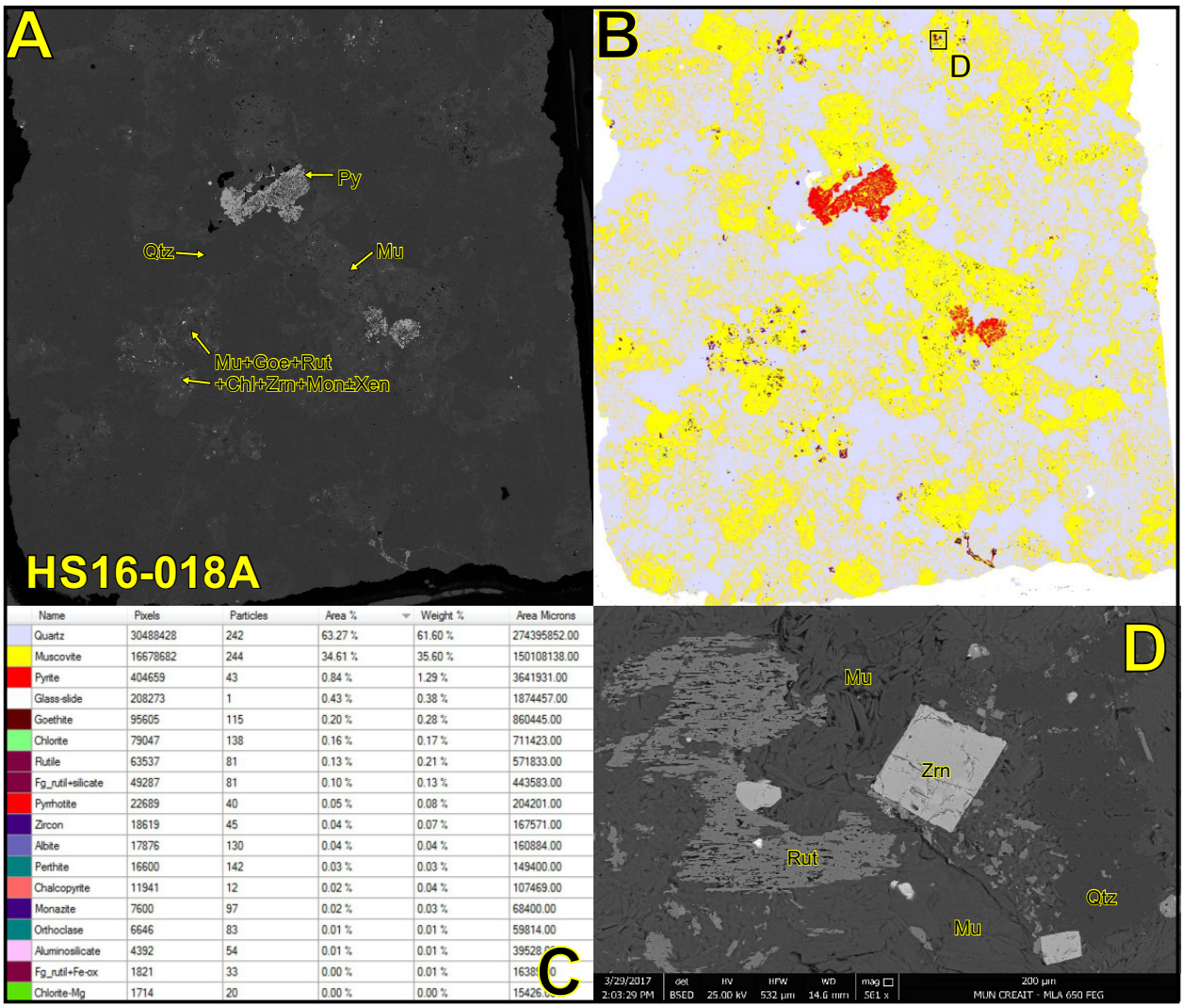

Name	Pixels	Particles	Area %	Weight %	Area Microns
Quartz	30488428	242	63.27 %	61.60 %	274395852.00
Muscovite	16678682	244	34.61 %	35.60 %	150108138.00
Pyrite	404659	43	0.84 %	1.29 %	3641931.00
Glass-slide	208273	1	0.43 %	0.38 %	1874457.00
Goethite	95605	115	0.20 %	0.28 %	860445.00
Chlorite	79047	138	0.16 %	0.17 %	711423.00
Rutile	63537	81	0.13 %	0.21 %	571833.00
Fg_rutil+silicate	49287	81	0.10 %	0.13 %	443583.00
Pyrrhotite	22689	40	0.05 %	0.08 %	204201.00
Zircon	18619	45	0.04 %	0.07 %	167571.00
Albite	17876	130	0.04 %	0.04 %	160884.00
Perthite	16600	142	0.03 %	0.03 %	149400.00
Chalcopyrite	11941	12	0.02 %	0.04 %	107469.00
Monazite	7600	97	0.02 %	0.03 %	68400.00
Orthoclase	6646	83	0.01 %	0.01 %	59814.00
Aluminosilicate	4392	54	0.01 %	0.01 %	39528.00
Fg_rutil+Fe-ox	1821	33	0.00 %	0.01 %	16385.00
Chlorite-Mg	1714	20	0.00 %	0.00 %	15426.00

Figure 7. *Electron microprobe MLA imagery for sample HS16-018A composed of bleached and fractured, muscovite–pyrite–rutile-altered monzogranite from near the centre of Yellow Fox Trench 3. A) BSE image of the thin section; B) MLA false-colour image of the mineralogy of the thin section showing subhedral spongy pyrite and the location of image D; C) Coloured legend for B; D) BSE image of a anhedral rutile accompanying muscovite and quartz and cubic zircon. Key: Qtz–quartz; Chl–chlorite; Mu–muscovite; Py–pyrite; Goe–goethite; Rut–rutile; Zrn–zircon; Mon–monazite; Xen–xenotime.*

Patches dominated by chlorite intergrown with muscovite + rutile + zircon + goethite ± xenotime (Figure 7D) are interpreted to represent the remnants of hydrothermally altered, intergrown primary biotite–hornblende–ilmenite–magnetite–zircon, such as those noted in miarolitic cavities in less strongly altered samples (*e.g.*, *see* HS16-017A: Sandeman *et al.*, 2018). In fresh samples, the ferromagnesian phases typically occur in small intercrystal druses or miarolitic cavities (Sandeman *et al.*, 2017). The rock consists of 63.3 wt. % quartz, 34.6% muscovite and <1% embayed and inclusion-rich pyrite with trace goethite, rutile and chlorite. All other phases identified in MLA analysis are in abundances of <0.1% (Figure 7). This sample also contains trace chalcopyrite, sphalerite, pyrrhotite, calcite and siderite.

Strongly Altered Stibnite-veined Monzogranite (*e.g.*, HS16-020B)

Sample HS16-020B is a sample of strongly altered, locally stibnite-veined monzogranite from Trench 1 (Figure 3) at the Yellow Fox showing. The wall rock to the vein is a chalky-orange-weathered, strongly sericite-altered, medium-grained monzogranite containing disseminated subhedral spongy pyrite (Figure 8). The altered rock is cut by anastomosing veinlets/fractures and patches filled with scorodite ($FeAsO_4 \cdot 2H_2O$; Plate 4C, D) and arsenopyrite partly altered to scorodite and goethite (Figure 8). The stibnite-dominated veins consist of stibnite intergrown with radial muscovite, and euhedral quartz and arsenopyrite

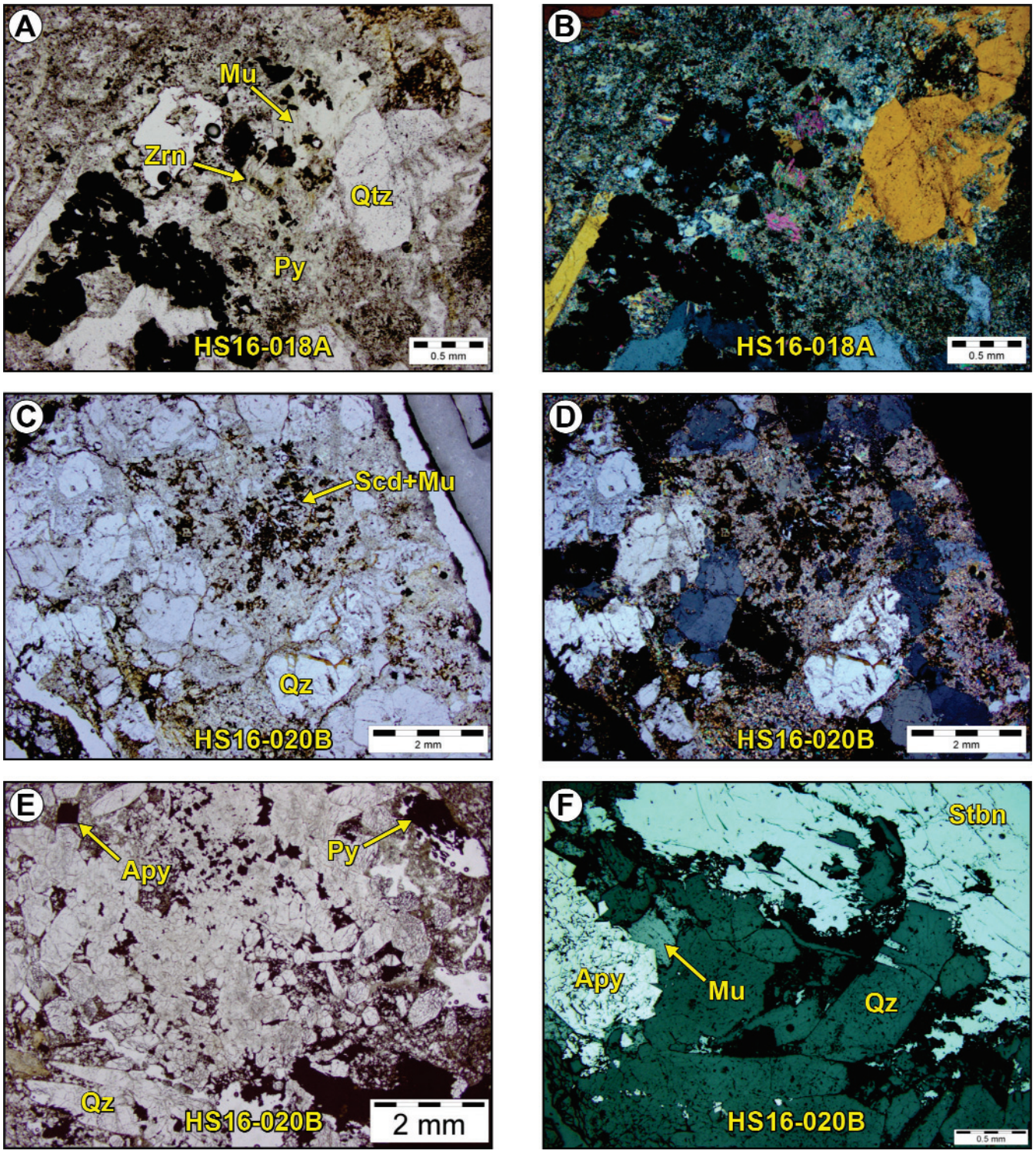

Plate 4. *Representative photomicrographs. A) Fractured muscovite–pyrite–rutile-altered monzogranite sample HS16-018A under ppl; B) Same field of sample HS16-18A view under crossed nicols. Note that this is a thick thin section; C) Stibnite–quartz–arsenopyrite-veined monzogranite sample HS16-020B under ppl; D) Same field of view of monzogranite sample HS16-020B under crossed nicols; E) Margin of stibnite–quartz–arsenopyrite vein and altered monzogranite sample HS16-020B under ppl; F) BSE image of intergrown stibnite, quartz, arsenopyrite and muscovite in sample HS16-020B. Key: Qz–quartz; Py–Pyrite; Apy–arsenopyrite; Stbn–stibnite; Mu–muscovite; Scd–scorodite; Zrn–zircon.*

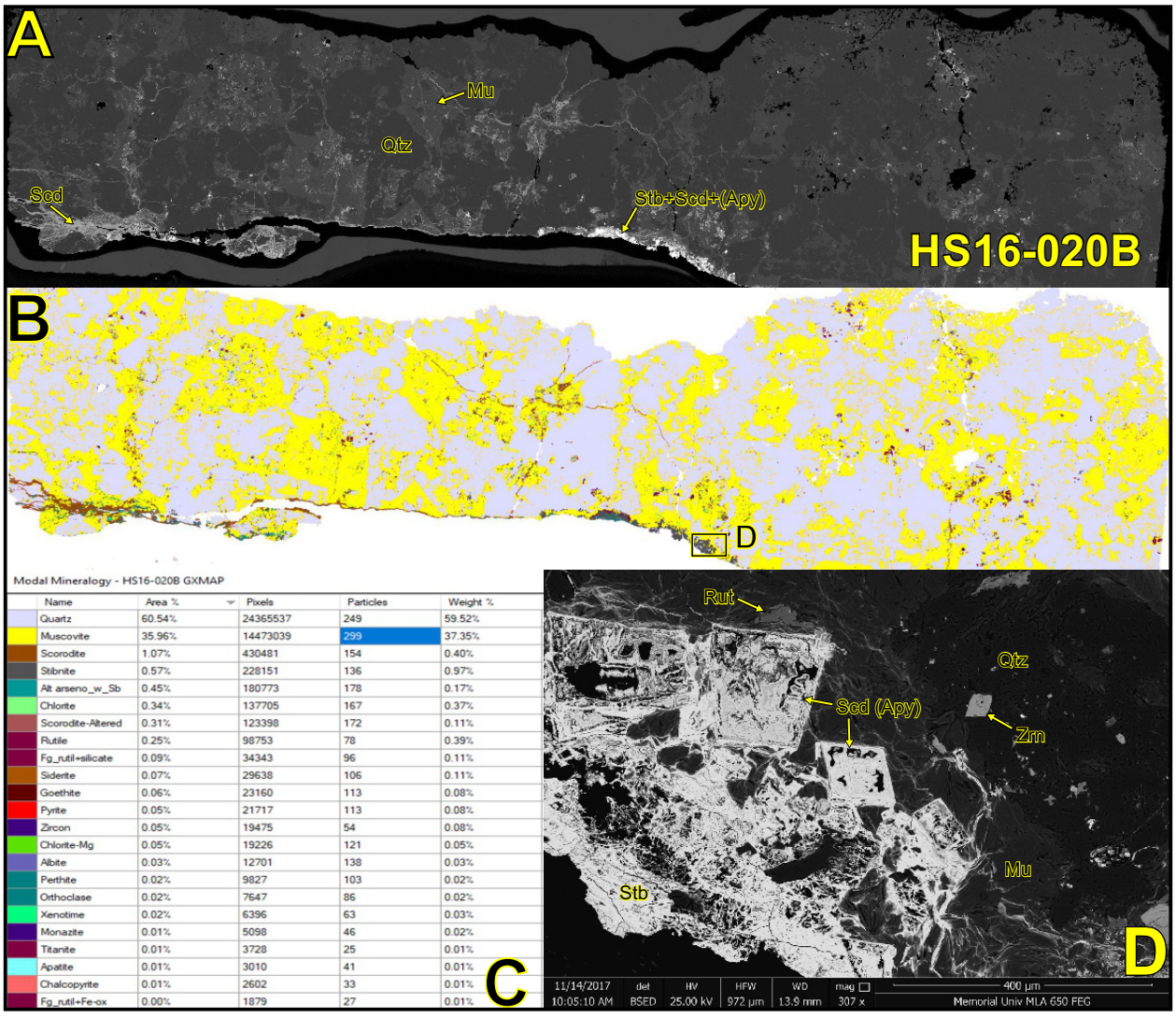

Figure 8. *Electron microprobe MLA imagery for sample HS16-020B composed of stibnite–quartz–arsenopyrite-veined monzogranite from the north central area of Yellow Fox Trench 1. A) BSE image of the thin section; B) MLA false-colour image of the mineralogy of the thin section showing the location of image D; C) Coloured legend for B; D) BSE image of the mineralized margin of the scorodite-altered stibnite–quartz–arsenopyrite vein in sample HS16-020B. Key: Qtz–quartz; Mu–muscovite; Apy–arsenopyrite; Goe–goethite; Rut–rutile; Zrn–zircon; Scd–scorodite; Stb–stibnite.*

(Figure 8; Plate 4E, F). The host rock consists of 60.5 wt. % quartz surrounded by 36.0%, radial and locally tabular muscovite that has essentially completely replaced all earlier feldspars in the rock (albite–orthoclase–perthite comprise 0.07%). Chalcopyrite, sphalerite, galena, siderite and calcite are present in trace amounts (Figure 8). The rock still locally retains a discernible granophyric texture.

LITHOGEOCHEMISTRY

Examination of the dataset reveals that weakly altered reddened monzogranite is chemically identical to the regional, background monzogranite samples, with no apparent depletion or enrichment in any element. Hence, these samples are all treated as fresh monzogranite unaffected by hydrothermal alteration and have major- and trace-element characteristics of calc-alkaline monzogranite (Figure 9A–C). Relative to these fresh rocks, bleached and fractured muscovite–pyrite–rutile-altered monzogranite exhibits elevated SiO_2 (74.5–78.4 *vs.* 70.3–74.0 wt. %), LOI (1.93–2.87 *vs.* 1.27–1.96 wt. %) and F (491–963 *vs.* 81–401 ppm), lower K_2O (3.44–4.82 *vs.* 4.70–4.99 wt. %), Ba (105–498 *vs.* 402–786 ppm), Rb (108–176 *vs.* 164–210 ppm), Sr (2–32 *vs.* 27–67 ppm), and Cs (0.7–3.1 *vs.* 1.8–6.2 ppm), and, signifi-

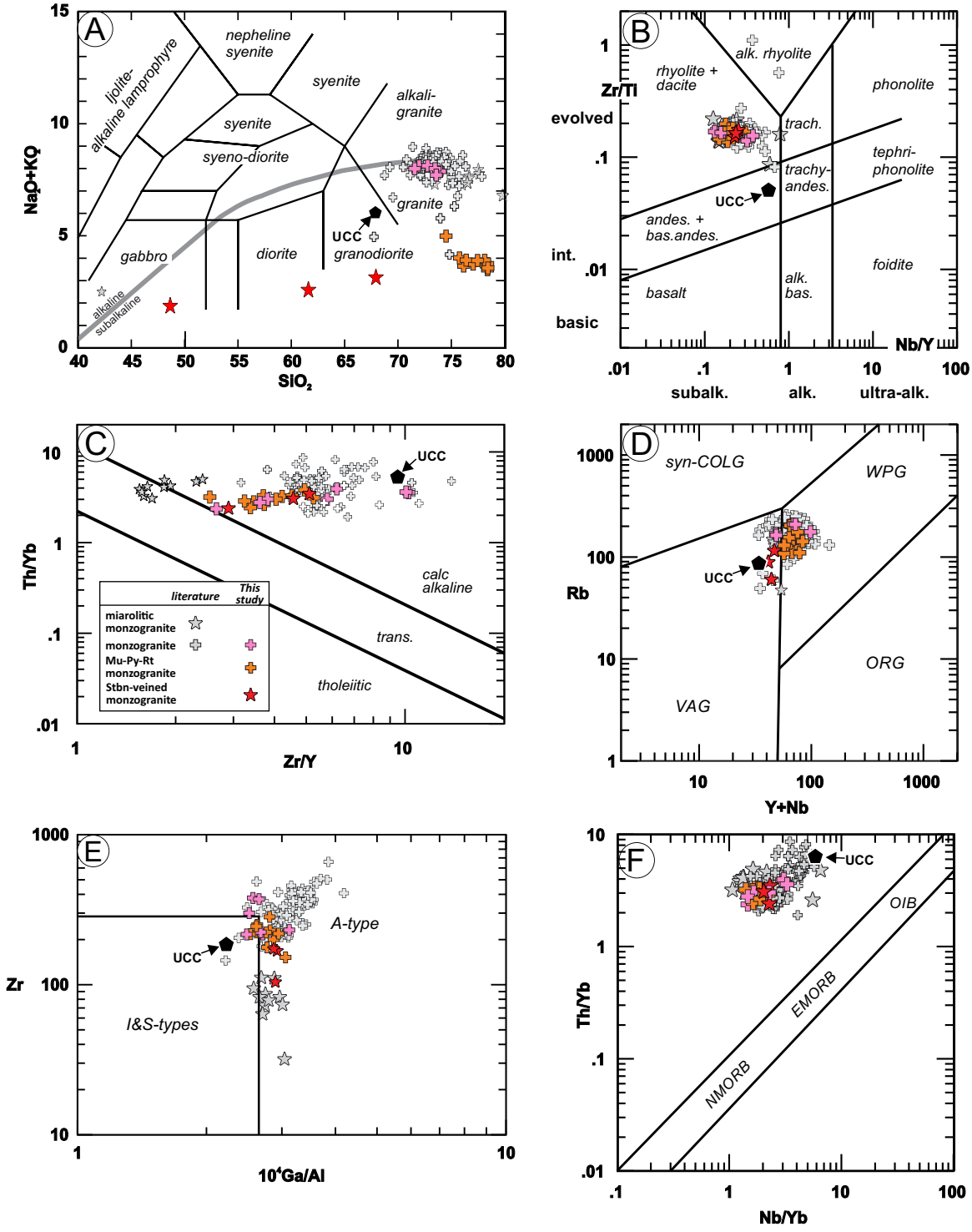

Figure 9. *Lithogeochemistry of the Yellow Fox samples including fresh (pink crosses), muscovite–pyrite–rutile-altered (orange crosses) and stibnite–quartz–arsenopyrite-veined monzogranite (red stars) compared to samples of regional Mount Peyton monzogranite (grey crosses: Dickson and Kerr, 2007; Sandeman, unpublished data, 2019). A) total alkalies* vs. *SiO_2 (after Wilson, 1989); B) Zr/Ti* vs. *Nb/Y classification diagram (after Pearce, 1996); C) Th/Yb* vs. *Zr/Y discrimination diagram (Ross and Bédard, 2009); D) Rb* vs. *Y+Nb paleotectonic discrimination diagram (Pearce* et al.*, 1984); E) Zr* vs. *10^4Ga/Al (Whalen* et al.*, 1987); F) Th/Yb* vs. *Nb/Yb (Pearce, 2008). Also shown are corresponding values for upper continental crust (UCC; Rudnick and Gao, 2003).*

cantly lower CaO (0.03–0.20 *vs.* 0.13–1.80 wt. %) and, in particular, Na_2O (0.04–0.31 *vs.* 2.97–3.50 wt. %). Many of the remaining major and incompatible trace elements in muscovite–pyrite–rutile-altered monzogranite have broadly similar concentrations as those in unaltered monzogranite, regardless of the intensity of alteration. Samples of the stibnite–quartz–arsenopyrite-veined monzogranite have the lowest concentrations of all of the major elements with the exception of FeO^T and LOI. The majority of incompatible trace elements, including the large ion lithophile elements (LILE) and the rare-earth elements (REE), also have substantially lower abundances in stibnite–quartz–arsenopyrite-veined monzogranite although their multi-element patterns are essentially identical. The precious metals Au and Ag, as well as many of the pathfinder elements (As, Sb, Cd) are all variably enriched in the stibnite-veined monzogranite relative to both the unaltered monzogranite and the bleached, fractured muscovite–pyrite–rutile-altered monzogranite.

Collectively, including all textural and chemical variants, the Yellow Fox samples are very similar to the regional samples of the MPIS monzogranite, and are transitional I to A-type granite (Pearce *et al.*, 1984; Whalen *et al.*, 1987; Figure 9D, E) having Th/Yb and Nb/Yb ratios characteristic of calc alkaline granite formed through subduction processes (Figure 9F; Pearce, 2008).

All samples, including the fresh, muscovite–pyrite–rutile-altered, and the stibnite-mineralized monzogranite samples exhibit broadly comparable REE patterns (Figure 10A) and multi-element patterns (Figure 10B) with LILE and light-REE enrichment (La_{CN}/Sm_{CN} = 2.56–3.18: CN denotes chondrite normalized) and weakly inclined middle to heavy REE segments (Gd_{CN}/Yb_{CN} = 1.15–1.72). They also exhibit modest Ba, Nb and Eu troughs and prominent negative Sr, P and Ti troughs (Figure 10B). Apart from variable relative abundances, little difference exists between the REE and multi-element patterns of the samples from the three monzogranite types (Table 1; Figure 10B), except that the muscovite–pyrite–rutile-altered monzogranite and the stibnite–arsenopyrite–quartz-veined monzogranite typically have deeper Ba, Nb, Sr, P, Ti and Eu troughs. The stibnite–arsenopyrite–quartz-veined monzogranite exhibits the lowest incompatible trace-element abundances of the three types (Figure 10A, B), although all samples have REE and multi-element patterns comparable to a field for 27 archival samples of MPIS granite (sensu lato; Dickson and Kerr, 2007; Sandeman, unpublished data, 2019).

ELEMENTS ASSOCIATED WITH MINERALIZATION

Figures 11 and 12 present the salient inter-element variations for specific elements of interest for samples collected from the Yellow Fox showing. Data from this study are compared to the available mineral-exploration industry data from the showing (Reid and Myllyaho, 2012), the regional MPIS monzogranite database (Dickson and Kerr, 2007; Sandeman *et al.*, 2017; Sandeman, unpublished data, 2019) and, the altered and precious-metal mineralized MPIS rocks from the Salmon River prospects (Tallman, 1991a; Evans, 1996; Evans and Dimmell, 2001; Evans *et al.*, 2001; Hoffe and Sparkes, 2003; House, 2003, 2005, 2007a, b; Sandeman *et al.*, 2017). The industry data mainly incorporate ICP and fire assay data for mineralized rocks from these areas, whereas the data of Hoffe and Sparkes (2003), Sandeman *et al.* (2017) and this study include a more complete and accurate lithogeochmical database. Figure 11 illustrates that, relative to the unaltered monzogranite, muscovite–pyrite–rutile-altered granite is characterized by variably elevated F (mean 655 *vs.* 256 ppm) and LOI (mean 2.38 *vs.* 1.49 wt. %). In contrast, the stibnite–quartz–arsenopyrite-veined monzogranite has broadly comparable F (mean 365 ppm), but strongly elevated LOI (mean 13.38 wt. %), relative to

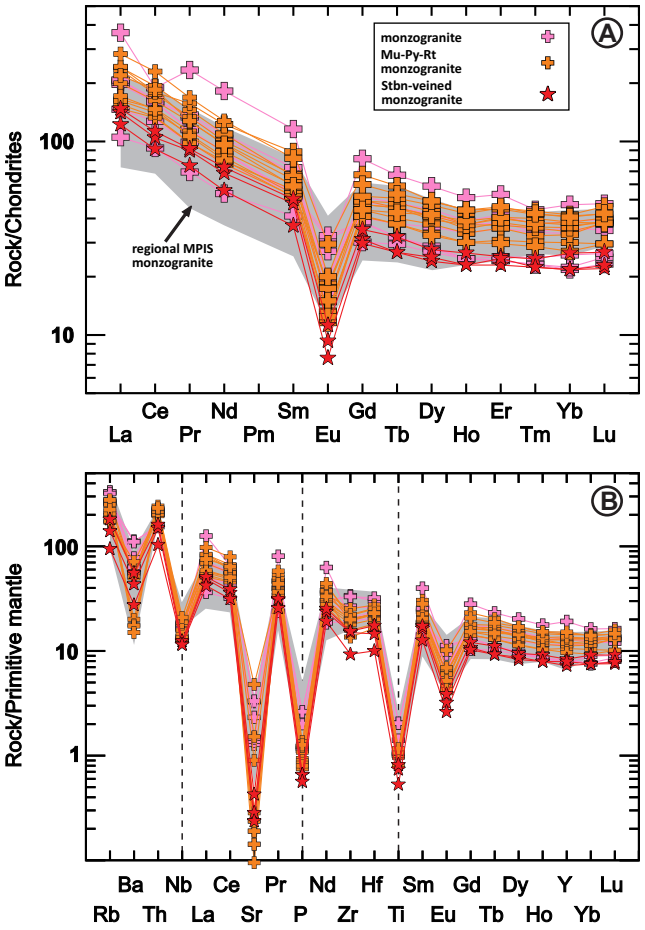

Figure 10. *A) Chondrite normalized rare-earth element plot and; B) Multi-element diagram for samples from the Yellow Fox showing. Normalization values are from Sun and McDonough (1989). Symbols and fields as in Figure 9.*

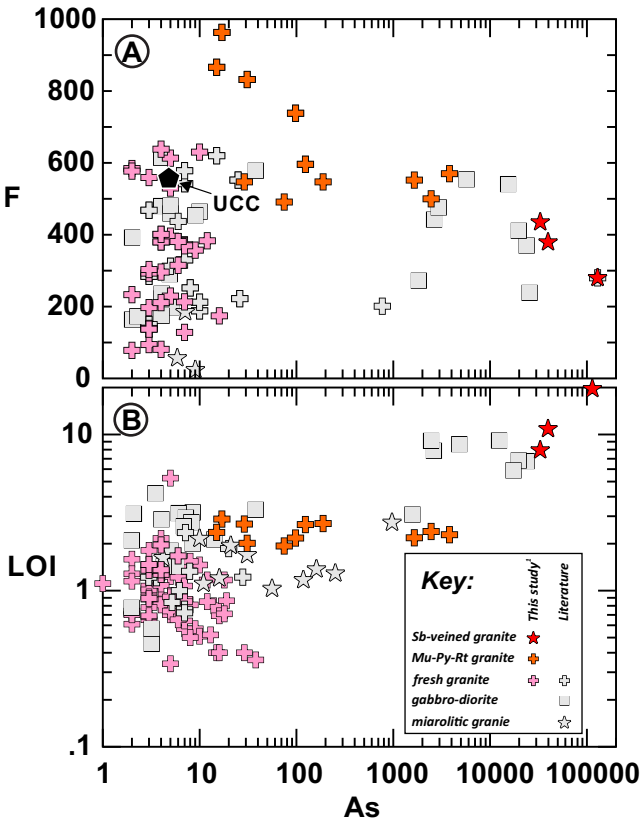

Figure 11. *Binary diagrams of (A) F* vs. *As and (B) LOI* vs. *As for samples from the Yellow Fox showing. Grey symbols represent samples from the MPIS-hosted, Salmon River and Slip mineralized zones (Tallman, 1991a; Evans, 1996; Evans and Dimmell, 2001; Evans* et al.*, 2001; Hoffe and Sparkes, 2003; House, 2003, 2005, 2007a, b; Sandeman* et al.*, 2017). UCC= upper continental crust composition from Rudnick and Gao (2003). Regional, fresh MPIS monzogranite analyses from this study supplemented with those from Dickson and Kerr (2007).*

unaltered monzogranite. Figure 12 shows that muscovite–pyrite–rutile-altered granite has variably elevated As, Au, Ag, Sb and Pb, but only weakly anomalous, Zn, Cu, Cd and Sn relative to unaltered monzogranite. Stibnite–arsenopyrite–quartz-veined monzogranite samples are the most enriched in As, Ag, Sb and Pb, and also contain anomalous Zn, Cu and Cd and weakly anomalous Sn (Figure 12). The granophile elements Mo and W are not enriched in hydrothermally altered samples relative to unaltered Yellow Fox monzogranite; however, these elements, as well as Sn, are all slightly elevated relative to average upper continental crust (UCC; Rudnick and Gao, 2003).

DISCUSSION

Field observations in 2016 and 2017, from mineral exploration trenches that are now backfilled and reclaimed, indicate that the Yellow Fox showing is a fracture-controlled, roughly north–south-trending, 30-m-wide by 100-m-long, hydrothermally altered and mineralized zone hosted by *ca.* 419 Ma plagioclase porphyritic, granophyric-textured, hornblende–biotite monzogranite of the MPIS. The core of the alteration zone is characterized by common, 5–20-cm-spaced, north-trending fractures (356°/80°E) around which strong bleaching and muscovite–pyrite–rutile alteration of the monzogranite has occurred. This core is mantled by reddened and weakly altered monzogranite. In the northernmost exposed bedrock (Trench 1), the fractured, muscovite–pyrite–rutile-altered monzogranite is cut by a ≤4-cm-wide stibnite–quartz–arsenopyrite vein (025°/86°E) and veinlets that have euhedral arsenopyrite, stibnite, muscovite and quartz, with mineralization also developed in the vein margins. The euhedral arsenopyrite grains are now largely replaced by a mixture of altered arsenopyrite, stibnite and scorodite, and the vein-marginal monzogranite is cut by scorodite–goethite-coated anastomosing fractures. The latter represent the products of late-stage, supergene alteration of the sulphide minerals and arsenopyrite in particular.

The fractured, muscovite–pyrite–rutile-altered monzogranite exhibits variable, but modestly anomalous, As, Au, Ag, Sb, Pb, and Cd relative to unaltered or weakly altered granite. In contrast, the stibnite–quartz–arsenopyrite-veins and altered wall-rock samples exhibit highly anomalous concentrations of As, Ag, Sb, Pb, Zn, Cd and weakly anomalous in Cu. Gold is apparently absent in the stibnite–quartz–arsenopyrite-veined monzogranite according to INAA data from this study (likely the result of gamma spectrum interference from antimony); however, fire assay data presented in Reid and Myllyaho (2012) suggest gold enrichment in their stibnite-veined monzogranite samples. The style and mineralogical characteristics of the alteration suggest the early infiltration of an acidic (H_2O-HF-HCL?), SiO_2 + K_2O + Fe + (S) + Au + Ag + Sb + As + Pb ± Zn–Cd–Cu–Sn(?)-bearing hydrothermal fluid along north-trending fractures in the monzogranite. This led to the destruction of feldspar, biotite and hornblende and the extensive replacement of the primary minerals in the monzogranite through the deposition of muscovite, pyrite and rutile. This event was followed by the development of a second suite of northeast-trending fractures, and the infiltration along those fractures of a second, H_2O + CO_2 + SiO_2 + K_2O + Fe + (S?) + Au + Sb + As + Ag + Pb + Zn + Cd ± Cu–Sn(?)-bearing hydrothermal fluid. Injection of this fluid led to the development of stibnite-quartz-arsenopyrite veins, accompanied by the deposition of euhedral stibnite, arsenopyrite and quartz in the vein wall rock. Subsequent supergene oxidation and hydration of the mineralization, possibly accompanying uplift and erosion, generated the young, anastomosing, scorodite–goethite-coated fractures.

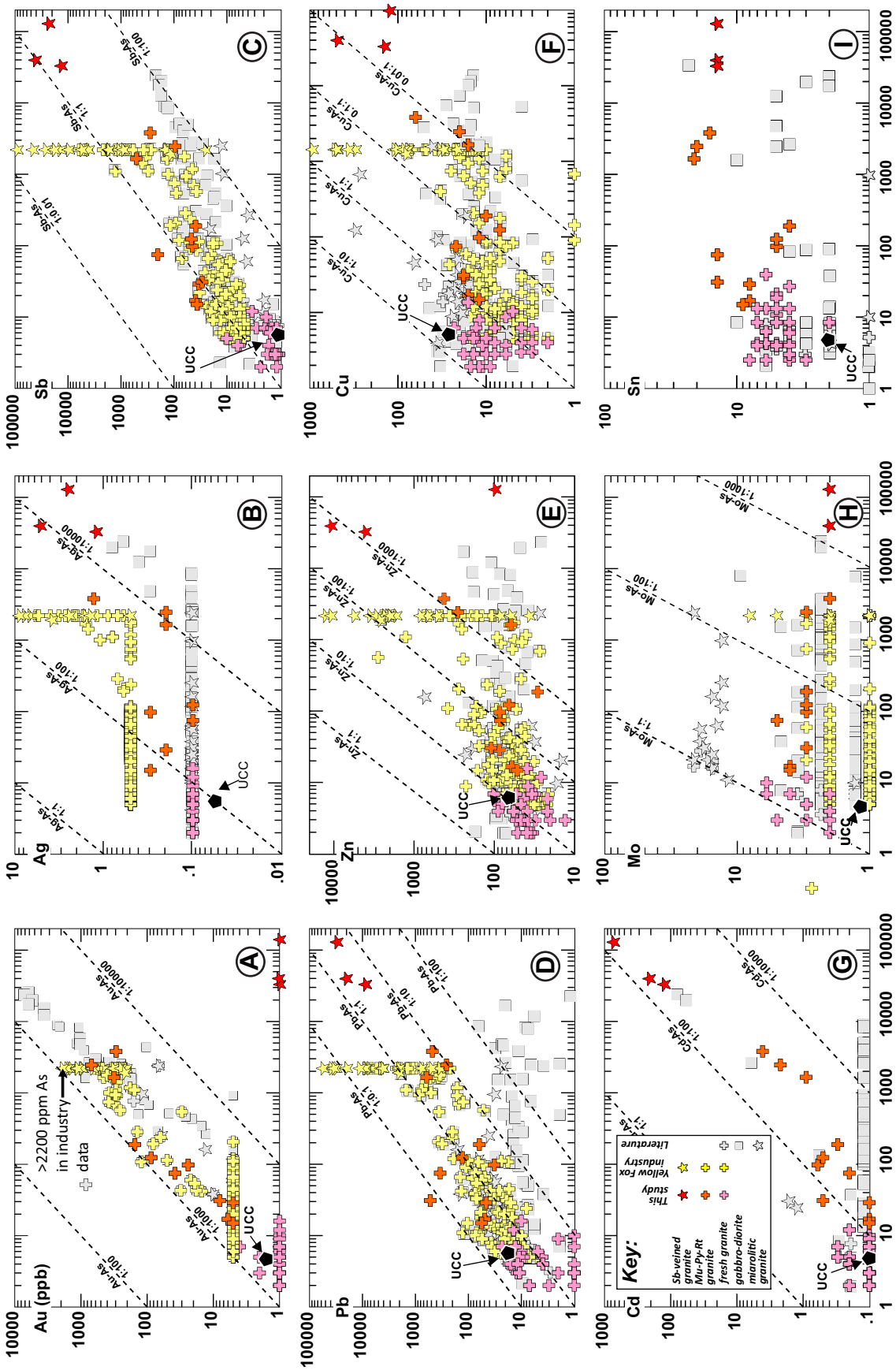

Figure 12. *Log-log plots for samples from the Yellow Fox showing. A) Au* vs. *As; B) Ag* vs. *As; C) Sb* vs. *As; D) Pb* vs. *As; E) Zn* vs. *As; F) Cu* vs. *As; G) Cd* vs. *As; H) Mo* vs. *As and I) Sn* vs. *As. Yellow symbols represent samples from a mineral-exploration industry assessment report (Reid and Myllahao, 2012). Grey symbols are samples from the Salmon River and Slip mineralized zones. Dashed lines represent lines of constant element/element ratios.*

The samples of muscovite–pyrite–rutile-altered monzogranite at Yellow Fox exhibit similar Au:As, Cd:As and perhaps Ag:As ratios to those of the intrusion-hosted, precious-metal-mineralized zones along the Salmon River; however their Sb:As and Pb:As distributions are distinct. Free gold has not been observed in thin section, or through MLA analysis, and may be hosted in the lattice of spongy pyrite. The elevated metal content of the stibnite–quartz–arsenopyrite-veined monzogranite is directly correlated with the volume % sulphide minerals. Preliminary electron microprobe analysis suggest the elevated As in the muscovite–pyrite–rutile-altered monzogranite may be hosted in arsenian pyrite.

The age of the mineralization is not known, but must be younger than the *ca.* 419 Ma age of the monzogranite. Fracturing, alteration and deposition of anomalous metals likely occurred in response to brittle failure of the rigid MPIS accompanying Early Devonian, north–northwest-directed thrusting (Dunning *et al.*, 1990; McNicoll *et al.*, 2006; Sandeman *et al.*, 2018), and imbrication of the adjacent, greenschist-facies grade metasedimentary rock-dominated sequences. The latter include the Badger Group in the west and northwest, and the Indian Islands Group strata to the east, which collectively form the country-rock carapace to the MPIS (*e.g.*, Dickson, 1993, 1996, 2006; Dickson *et al.*, 2000, 2007; O'Brien, 2003; Sandeman *et al.*, 2018). Termination of Early Devonian ductile deformation in the northern Exploits Subzone has been precisely constrained at 415–410 Ma on Birchy Island in the Bay of Exploits, 48 km to the north–northwest (McNicoll *et al.*, 2006). The brittle fracturing of the MPIS that generated the fracturing and alteration at Yellow Fox, and the Salmon River mineralized zones may have been synchronous with, or postdated, that final ductile deformation event. Direct geochronological data for the age of alteration and mineralization are necessary to resolve this temporal issue.

ACKNOWLEDGMENTS

Gerry Hickey is thanked for logistical assistance. Cameron Peddle provided very capable field assistance in 2016. Thanks to John Hinchey and Greg Sparkes for insightful reviews of this contribution.

REFERENCES

Anderson, F.D. and Williams, H.
1970: Geology of Gander Lake [2D] west half, Newfoundland. Geological Survey of Canada, "A" Series Map 1195A.

Baird, D.M., Moore, J.C.G., Scott, H.S. and Walker, W.
1951: Reconnaissance geology of east-central Newfoundland between Sir Charles Hamilton Sound and Bay d'Espoir. Unpublished report, Photographic Survey Corporation, Toronto, 155 pages. [NFLD(446)]

Barbour, D.M. and Churchill, R.A.
1999: First year assessment report on geological, geochemical, geophysical and diamond drilling exploration for licence 6101m on claims in The Outflow area, Gander Lake, central Newfoundland. Newfoundland and Labrador Geological Survey, Assessment File 2D/15/0362, 1999, 121 pages.

2004: Second, third, and sixth year assessment report on prospecting, mapping and geochemical sampling for the Mustang Trend Properties, map staked licenses 8252M, 8253M, 8254M, 6101M, 7677M, 8255M, 9646M, 9650M and 9788M; NTS sheets 02E02, 02E07, 02D05, 02D06, 02D11, 02D12, 02D13, 02D14, & 02D15, Botwood Basin, central Newfoundland. Newfoundland and Labrador Geological Survey, Assessment File 2D/15/2893, 413 pages.

Bell, K., Blenkinsop, J. and Strong, D. F.
1977: The geochronology of some granitic bodies from eastern Newfoundland and its bearing on Appalachian evolution. Canadian Journal of Earth Sciences, Volume 14, pages 456-476.

Blackwood, R.F.
1982: Gander (Mount Peyton E.), Newfoundland. Map 80-198. Scale: 1:50 000. *In* Geology of the Gander Lake (2D/15) and Gander River (2E/2) area. Government of Newfoundland and Labrador, Department of Mines and Energy, Mineral Development Division, Report 82-04, 63 pages, enclosures (2 maps, cross-section). GS# NFLD/1312b.

Boyce, W.D. and Ash, J.S.
1994: New Silurian-Devonian [?] faunas from the Gander (NTS 2D/15) and Botwood (NTS 2E/3) map areas. *In* Current Research. Government of Newfoundland and Labrador, Department of Mines and Energy, Geological Survey Branch, Report 94-1, pages 53-63.

Boyce, W.D. and Dickson, W.L.
2006: Recent fossil finds in the Indian Islands Group, central Newfoundland. *In* Current Research. Government of Newfoundland and Labrador, Department of Natural Resources, Geological Survey, Report 06-1, pages 221-231.

Clarke, J.
1996: Precious metal properties available for option: The Greenwood Pond and Indian Arm properties. FOREX Resources, unpublished company report number 2, 28 pages.

Colman-Sadd, S.P., Hayes, J.P. and Knight, I.
1990: Geology of the Island of Newfoundland. Newfoundland and Labrador Geological Survey, Map 90-001.

Currie, K.L.
1993: Ordovician-Silurian stratigraphy between Gander Bay and Birchy Bay, Newfoundland. Geological Survey of Canada, Paper 93-1D, pages 11-18.

1995: The northeastern end of the Dunnage Zone in Newfoundland. Atlantic Geology, Volume 31, pages 25-38.

Davenport, P.H. and Nolan, L.W.
1989: Mapping the regional distribution of gold in Newfoundland using lake sediment geochemistry. *In* Current Research. Government of Newfoundland and Labrador, Department of Mines, Geological Survey, Report 89-1, pages 259-266.

Dickson, W.L.
1993: Geology of the Mount Peyton map area (NTS 2D/14), central Newfoundland. *In* Current Research. Government of Newfoundland and Labrador, Department of Mines and Energy, Geological Survey Branch, Report 93-1, pages 209-220.

1994: Geology of the southern portion of the Botwood map area (NTS 2E/3), north-central Newfoundland. *In* Current Research. Government of Newfoundland and Labrador, Department of Mines and Energy, Geological Survey Branch, Report 94-1, pages 101-116.

1996: Geochemical sample sites in the Mount Peyton (2D/14) map area, central Newfoundland. Map 96-27. Scale: 1:50 000. *In* Whole-rock Geochemical and Field Data from the Mount Peyton Intrusive Suite, the Great Bend Complex and Miscellaneous Rocks, Central Newfoundland (NTS Map Areas 2D/11E, 2D/14, 2E/3 and Parts of 2D/13 and 2D/15). Government of Newfoundland and Labrador, Department of Mines and Energy, Geological Survey, Open File NFLD/2614.

2006: The Silurian Indian Islands Group and its relationships to adjacent units. *In* Current Research. Government of Newfoundland and Labrador, Department of Natural Resources, Geological Survey, Report 06-1, pages 1-24.

Dickson, W.L. and Kerr, A.
2007: An updated database of historic geochemical data for granitoid plutonic suites of Newfoundland. Government of Newfoundland and Labrador, Department of Natural Resources, Geological Survey, Open File NFLD/2957.

Dickson, W.L., O'Brien, B.H. and Colman-Sadd, S.P.
2000: Geology of the Botwood map area (NTS 2E/3), central Newfoundland. Map 2000-11, Version 2.0. Government of Newfoundland and Labrador, Department of Mines and Energy, Geological Survey, Open File 2E/03/1067.

Dickson, W.L., McNicoll, V.J., Nowlan, G.S. and Dunning, G.R.
2007: The Indian Islands Group and its relationships to adjacent units: recent data. *In* Current Research. Government of Newfoundland and Labrador, Department of Natural Resources, Geological Survey, Report 07-1, pages 1-9.

Doublier, M.P., Roache, A. and Potel, S.
2010: Application of SWIR spectroscopy in very low-grade metamorphic environments: A comparison with XRD methods. Geological Survey of Western Australia Record 2010/7, 61 pages (http://www.dmp.wa.gov.au/7119.aspx).

Duke, E.F.
1994: Near infrared spectra of muscovite, Tschermak substitution, and metamorphic reaction process: Implications for remote sensing. Geology, Volume 22, pages 621-624, doi: 10.1130/0091-7613(1994)022<0621:NISOMT>2.3.CO;2.

Dunning, G.R.
1992: U/Pb Geochronological research agreement. Final report for the Newfoundland Department of Mines and Energy, Newfoundland Mapping Section. Geological Survey, Newfoundland Department of Mines and Energy, unpublished report. [NFLD/2937]

1994: U/Pb Geochronological research agreement. Final report for the Newfoundland Department of Mines and Energy, Newfoundland Mapping Section. Geological Survey, Newfoundland Department of Mines and Energy, unpublished report. [NFLD2939]

Dunning, G.R. and Manser, K.
1993: U/Pb Geochronological research agreement. Final report for the Newfoundland Department of Mines and Energy, Newfoundland Mapping Section. Geological Survey, Newfoundland Department of Mines and Energy, unpublished report. [NFLD/2938]

Dunning, G.R., O'Brien, S.J., Colman-Sadd, S.P., Blackwood, R.F., Dickson, W.L., O'Neill, P.P. and T.E. Krogh
1990: Silurian Orogeny in the Newfoundland Appalachians. Journal of Geology, Volume 98, pages 895-913.

Evans, D.T.W.
1996: Epigenetic gold occurrences, eastern and central Dunnage Zone, Newfoundland. Government of Newfoundland and Labrador, Department of Mines and Energy, Geological Survey, Mineral Resources Report 9, 135 pages.

Evans, D.T.W. and Dimmell, P.M.
2001: First year assessment report on prospecting and geochemical exploration for licence 7093M on claims in the Shirley Lake area, central Newfoundland. Newfoundland and Labrador Geological Survey, Assessment File 2E/03/1478, 39 pages.

Evans, D.T.W., DuPre, D.G., Dimmell, P.M. and Lewis, G.
2001: First year assessment report on prospecting and geochemical exploration for licence 7022M on claims in the Shirley Lake area, central Newfoundland, 2 reports. Newfoundland and Labrador Geological Survey, Assessment File 2E/03/1366, 66 pages.

Evans, D.T.W., Hayes, J.P. and Blackwood, R.F.
1992: Gander River, Newfoundland. Government of Newfoundland and Labrador, Department of Mines and Energy, Geological Survey Branch, Open File 2E/02/0839.

Evans, D.T.W., and Wilson, M.
1994: Epigenetic gold occurrences in the eastern dunnage zone, Newfoundland: Preliminary stable-isotope results. *In* Current Research. Government of Newfoundland and Labrador, Department of Mines and Energy, Geological Survey Branch, Report 94-1, pages 211-223.

Finch, C., Roldan, R., Walsh, L., Kelly, J. and Amor, S.
2018: Analytical methods for chemical analysis of geological materials. Government of Newfoundland and Labrador, Department of Natural Resources, Geological Survey, Open File NFLD/3316, 67 pages.

Hoffe, C.K.
2003: A detailed examination of the relationships between intrusive phases of the Neyles Brook quarry, Mount Peyton. Unpublished B.Sc. thesis, Memorial University of Newfoundland, St. John's, Newfoundland, 87 pages.

Hoffe, C.K. and Sparkes, B.A.
2003: Fourth year assessment report on geological and geochemical exploration for licence 6610M on claims in the Neyles Brook area, central Newfoundland. Rubicon Minerals Corporation and Quest Incorporated. Unpublished report, 85 pages. [GSB# 002E/03/1367]

House, S.
2003: Second year assessment report on prospecting and geochemical exploration for licence 7975M on claims in the Salmon River area, central Newfoundland. Newfoundland and Labrador Geological Survey, Assessment File NFLD/2842, 25 pages.

2005: First, third and fifth year assessment report on prospecting and geochemical exploration for licences 7093M, 8261M, 8361M and 9808M-9809M on claims in the Shirley Lake area, near Glenwood, central Newfoundland. Rubicon Minerals Corporation and Black Bart Prospecting Incorporated. Unpublished report, 95 pages. [GSB# NFLD/2958]

2007a: Fourth, sixth and eighth year assessment report on prospecting and geochemical and diamond drilling exploration for licences 7022M, 7093M, 9808M and 10462M on claims in the Shirley Lake area, central Newfoundland. Newfoundland and Labrador Geological Survey, Assessment File NFLD/3062, 107 pages.

2007b: Eighth year assessment report on geological and geochemical exploration for licence 6610M on claims in the Indian Arm Pond area, southeast of Notre Dame Junction, Newfoundland. Newfoundland and Labrador Geological Survey, Assessment File 2E/03/1551, 46 pages.

House, S. and McConnell, D.
2003: First and second year assessment report on prospecting and geochemical and geophysical exploration for licences 7925M, 7928M, 7976M and 8260M8261M on claims in the Salmon River area, near Glenwood, central Newfoundland, 2 reports. Newfoundland and Labrador Geological Survey, Assessment File 2D/0448, 60 pages.

Hynes, G.F. and Rivers, T.
2002: A study of the metamorphic aureole of the Mount Peyton intrusive suite, Dunnage Zone, central Newfoundland. *In* Current Research. Government of Newfoundland and Labrador, Department of Natural Resources, Geological Survey, Report 02-1, pages 53-65.

Kerr, A., Rafuse, H., Sparkes, G., Hinchey, J. and Sandeman, H.
2011: Visible/infrared spectroscopy (VIRS) as a research tool in economic geology: background and pilot studies from Newfoundland and Labrador. *In* Current Research. Government of Newfoundland and Labrador, Department of Natural Resources, Geological Survey, Report 11-1, pages 145-166.

Lake, J. and Wilton, D.H.C.
2006: Structural and stratigraphic controls on mineralization at the Beaver Brook antimony deposit, central Newfoundland. *In* Current Research. Government of Newfoundland and Labrador, Department of Natural Resources, Geological Survey, Report 06-1, pages 135-146.

McNicoll, V.J., Squires, G.C., Wardle, R.J., Dunning, G.R. and O'Brien, B.H.
2006: U–Pb geochronological evidence for Devonian deformation and gold mineralization in the eastern Dunnage Zone, Newfoundland. *In* Current Research. Government of Newfoundland and Labrador, Department of Natural Resources, Geological Survey, Report 06-1, pages 45-60.

Miller, H. G. and Thakwalakwa, S.A.M.
1992: A geophysical and geochemical interpretation of the configuration of the Mount Peyton Complex, central Newfoundland. Atlantic Geology, Volume 28, pages 221-231.

Moore, P.J. and Smith, P.A.,
2003: First, second, third and fourth year assessment report on prospecting and geochemical and geophysical exploration for licences 7180M-7181M, 7912M, 8477M, 8600M-8606M and 8608M-8609M on claims in the Gander River area, central Newfoundland, 2 reports. Newfoundland and Labrador Geological Survey, Assessment File NFLD/2848, 417 pages.

O'Brien, B.H.
2003: Simplified geology of the northeast Dunnage Zone between Halls Bay and Hamilton Sound, Notre Dame Bay, Newfoundland. Map 2001-041. Government of Newfoundland and Labrador, Department of Mines and Energy, Geological Survey Branch, Open File 2E/1247.

O'Driscoll, J.M. and Wilton, D.H.C.
2005: Preliminary geochronological, geochemical and isotopic studies of auriferous systems in the Botwood Basin and environs, central Newfoundland. *In* Current Research. Government of Newfoundland and Labrador, Department of Natural Resources, Geological Survey, Report 05-1, pages 207-222.

O'Reilly, D.F. and Churchill, R.A.
2004: Third year assessment report on linecutting and soil sampling for map staked licenses 8252M (Glenwood Fault), 10408M (Clark's Brook North) and 10409M (Clark's Brook South), Mustang Trend Project; Botwood Basin, central Newfoundland, NTS sheets 02D1, 02D14 and 02D15. Newfoundland and Labrador Geological Survey, Assessment File NFLD/2894, 75 pages.

O'Reilly, D., O'Driscoll, J., Winter, L. and Churchill, R.A.
2008: First year assessment report on geochemical exploration for licences 13256M-13259M on claims in the Glenwood and Northwest Gander River areas, central Newfoundland. Newfoundland and Labrador Geological Survey, Assessment File 2D/0718, 52 pages.

O'Reilly, D., O'Driscoll, J., Devereaux, A. and Churchill, R.
2010: First year assessment report on geological, geochemical, geophysical and trenching exploration for licenses 13256M, 13259M, 15198M, 15925M and 15926M on claims in the Glenwood and Northwest Gander River areas, central Newfoundland, 3 reports. Newfoundland and Labrador Geological Survey, Assessment File 2D/0763, 84 pages.

Pearce, J.A.
1996: A user's guide to basalt discrimination diagrams. Geological Association of Canada, Short Course Notes, Volume 12, pages 79-113.

2008: Geochemical fingerprinting of oceanic basalts with applications to ophiolite classification and the search for Archean oceanic crust. Lithos, Volume 100, pages 14-48.

Pearce, J.A., Harris, N.B.W. and Tindle, A.G.
1984: Trace element discrimination diagrams for the tectonic interpretation of granitic rocks. Journal of Petrology, Volume 25, pages 956-983.

Pollock, J.C., Wilton, D.H.C., van Staal C.R. and Morrissey, K.D.
2007: U–Pb detrital zircon geochronological constraints on the Early Silurian collision of Ganderia and Laurentia along the Dog Bay Line: The terminal Iapetan suture in the Newfoundland Appalachians. American Journal of Science, Volume 307, pages 399-433, doi 10.2475/02.2007.04.

Piasecki, M.A.J.
1993: Tectonics along the Dog Bay Line – a Silurian terrane boundary in northeastern Newfoundland. *In* Current Research, Part E. Geological Survey of Canada, Paper 93-E1, pages 291-298.

Quinlan, E.
2009: First year assessment report on prospecting and geochemical exploration for licence 15196M on claims in the Neyles Brook area, central Newfoundland. Newfoundland and Labrador Geological Survey, Assessment File 2E/03/1645, 46 pages.

Quinlan, L.
2013: First year assessment report on prospecting and geochemical exploration for licence 20334M on claims in the Clarkes Brook area, central Newfoundland. Newfoundland and Labrador Geological Survey, Assessment File 2D/14/0792, 12 pages.

Reid, W. and Myllyaho, J.
2012: First year assessment report on prospecting and geochemical and trenching exploration for licences 19103M, 19120M, 19318M and 19493M on claims in the Gander Lake area, central Newfoundland. Newfoundland and Labrador Geological Survey, Assessment File 2D/0779, 48 pages.

Reynolds, P.H., Taylor, K.A. and Morgan, W.R.
1981: ^{40}Ar–^{39}Ar ages from the Botwood–Mount Peyton region, Newfoundland: Possible paleomagnetic implications. Canadian journal of Earth Sciences, Volume 18, pages 1850-1855.

Ross, P. and Bédard, J.H.
2009: Magmatic affinity of modern and ancient subalkaline volcanic rocks determined from trace-element discriminant diagrams. Canadian Journal of Earth Sciences, Volume 46, pages 823-839.

Rudnick, R.L. and Gao, S.
2003: Composition of the continental crust. *In* Treatise on Geochemistry. *Edited by* H.D. Holland and K.K. Turekian. *In* The Crust, Volume 3. *Edited by* R.L. Rudnick. Elsevier-Permagon, Oxford, pages 1-64.

Sandeman, H.A.I., Dunning, G.R., McCullough, C.K. and Peddle, C.
2017: U–Pb geochronology, petrogenetic relationships and intrusion-related precious-metal mineralization in the northern Mount Peyton intrusive suite: Implications for the origin of the Mount Peyton trend, central Newfoundland (NTS 2D/04). *In* Current Research. Government of Newfoundland and Labrador, Department of Natural Resources, Geological Survey, Report 17-1, pages 189-217.

Sandeman, H.A.I., Peddle, C. and Newman, R.
2018: Beaver Brook antimony mine revisited: an update on operations and new structural and geological observations. *In* Current Research. Government of Newfoundland and Labrador, Department of Natural Resources, Geological Survey, Report 18-1, pages 123-152.

Spurrell, C.
2017: Documentation of the Yellow Fox antimony–silver–gold showing, central Newfoundland. Unpublished B.Sc. thesis, Memorial University of Newfoundland and Labrador, St. John's, 48 pages.

Squires, G.C.
2005: Gold and antimony occurrences of the Exploits Subzone and Gander Zone: A review of recent discoveries and their interpretation. *In* Current Research. Government of Newfoundland and Labrador, Department of Natural Resources, Geological Survey, Report 05-1, pages 223-237.

Strong, D.F.
1977: The Mount Peyton batholith, central Newfoundland: A biomodal calc-alkaline suite. Canadian Journal of Earth Sciences, Volume 20, pages 119-138.

Strong, D.F. and Dupuy, C.
1982: Rare earth elements in the bimodal Mount Peyton batholith: Evidence for crustal anatexis by mantle-derived magma. Canadian Journal of Earth Sciences, Volume 19, pages 308-315.

Sun, S.S. and McDonough, W.F.
1989: Chemical and isotopic systematics of oceanic basalts: implications for mantle composition and processes. *In* Magmatism in the Ocean Basin. *Edited by* A.D. Saunders and M.J. Norry. Geological Society of London, Special Publication 42, pages 313-345.

Tallman, P.
1990: First year assessment report on geological, geochemical, geophysical and trenching exploration for the Noront-Grub Line S project for licence 3544 on claim block 15841 and licence 3856 on claim blocks 12939, 15834, 15844-15845, 16953, 16962 and 16964-16966 in the Salmon River area, Newfoundland. Newfoundland and Labrador Geological Survey, Assessment File NFLD/1968, 135 pages.

1991a: Second year assessment report on geological, geochemical, geophysical and diamond drilling exploration for the Mount Peyton project for licence 3544 on claim block 15841 in the Salmon River area, Newfoundland. Newfoundland and Labrador Geological Survey, Assessment File 2D/0247, 98 pages.

1991b: The Hunan Line discoveries: antimony mineralization in central Newfoundland. *In* Ore Horizons, Volume 1. Government of Newfoundland and Labrador, Department of Mines and Energy, Geological Survey Branch, pages 11-21.

Tallman, P. and Evans, D.T.W.
1994: Geology of stibnite mineralization at the Hunan Line prospects, central Newfoundland. *In* Current Research. Government of Newfoundland and Labrador, Department of Mines and Energy, Geological Survey Branch, Report 94-1, pages 263-271.

Valverde-Vaquero, P., van Staal, C.R., McNicoll, V., and Dunning, G.R.
2006: Mid–Late Ordovician magmatism and metamorphism along the Gander margin in central Newfoundland. Journal of the Geological Society, Volume 163, pages 347-362.

van Staal, C.R., Zagorevski, A., McNicoll, V.J. and Rogers, N.,
2014: Time-transgressive Salinic and Acadian orogenesis, magmatism, and Old Red Sandstone sedimentation in Newfoundland. Geoscience Canada, Volume 41, pages 138-164.

Wanless, R.K., Stevens, R.D., Lachance, G.R. and Edmonds, C.M.
1967: Age determinations and geological studies: KAr isotopic ages, Report 7. Geological Survey of Canada, Report 66-17, 120 pages.

Whalen, J.B., Currie, K.L. and Chappell, B.W.
1987: A-type granites: geochemical characteristics, discrimination and petrogenesis. Contributions to Mineralogy and Petrology, Volume 95, pages 407-419.

Whitney, D.L. and Evans, B.W.
2010: Abbreviations for names of rock-forming minerals. American Mineralogist, Volume 95, pages 185-187.

Williams, H.
1962: Botwood, west half, map area, Newfoundland, 2E/W. Geological Survey of Canada, Paper 62-09, 21 pages.

1993: Stratigraphy and structure of the Botwood Belt and definition of the Dog Bay Line in northeastern Newfoundland. *In* Current Research, Part D. Geological Survey of Canada, Paper 93-1D, pages 19-27.

Williams, H., Currie, K.L. and Piasecki, M.A.J.
1993: The Dog Bay Line: A major Silurian tectonic boundary in northeast Newfoundland. Canadian Journal of Earth Sciences, Volume 30(12), pages 2481-2494.

Williams, H. (ed.)
1995: Geology of the Appalachian-Caledonian Orogen in Canada and Greenland; Geological Survey of Canada, Geology of Canada, no. 6 (also Geological Society of America, The Geology of North America, v. F-1; 944 pages.

Wilson, B.M.
1989: Igneous Petrogenesis a Global Tectonic Approach. Unwin and Hyman, London, 466 pages.